



IUSM-Purdue TREAT-AD Center Target Enabling Component

INPP5D (SHIP1) Chemical Probe

NCBI Gene ID / UniProt ID	3635/Q92835
Authors	Timothy I Richardson
Collaborating Authors	Cynthia D Jesudason, Emily R Mason, Shaoyou Chu, Adrian L Oblak, June Javens-Wolfe, Mustapha Moussaif, Greg Durst, Philip Hipkind, Daniel E. Beck, Jiajun Dong, Ovin Amarasinghe, Zhong-Yin Zhang, Adam K Hamdani, Kratika Singhal, Andrew D Mesecar, Sarah Souza, Marlene Jacobson, Jerry Di Salvo, Disha M Soni, Murugesh Kandasamy, Andrea R Masters, Sara K Quinney, Suzanne Doolen, Hasi Huhe, Stacey J Sukoff Rizzo, Bruce T Lamb, Alan D Palkowitz
Date Approved by Admin Core	February 13, 2024
Document version	4.0
Document version date	February 22, 2024
Citation	https://doi.org/10.5281/zenodo.723178 Now published in <i>Alzheimer's Dement.</i> 2023; 9:e12429. https://doi.org/10.1002/trc2.12429
Affiliations	Indiana University School of Medicine, Purdue University, Evotec, Lgenia, Indiana Biosciences Research Institute, University of Pittsburgh School of Medicine

1 BACKGROUND

Alzheimer's disease (AD) is a progressive neurodegenerative disorder that is characterized by the accumulation of abnormal protein aggregates, including A β plaques and tau tangles, in the brain. Gradual neurodegeneration leads to cognitive decline, memory loss, and behavioral changes. Specific triggers and mechanisms are not yet fully understood; however, they likely result from a complex interplay of genetics, environment, and lifestyle. Genome-wide association studies (GWAS), whole genome sequencing, and gene-expression network analyses comparing normal aged brain to samples from patients with Late-onset Alzheimer's disease (LOAD) have identified protective and risk genes involved in microglia function and neuroinflammation¹⁻⁴. Target selection and validation based on these studies remains a challenge. It is often unclear if a successful therapeutic intervention would require target upregulated or downregulated and the timing of such interventions remain unclear.

The Target Enablement to Accelerate Therapy Development for Alzheimer's Disease (TREAT-AD) centers were established to provide high-quality research tools and technologies to validate and advance the next generation of drug targets for Alzheimer's Disease (AD)⁵. Data, methods, and computational and experimental tools are being disseminated openly and free-of-charge to the broader research community for use in drug discovery and in research to better understand the complex biology of AD. Resources are made available in a Target Enablement Package (TEP) at the AD Knowledge Portal (<https://adknowledgeportal.synapse.org/Explore/Target%20Enabling%20Resources>). Here the IUSM-

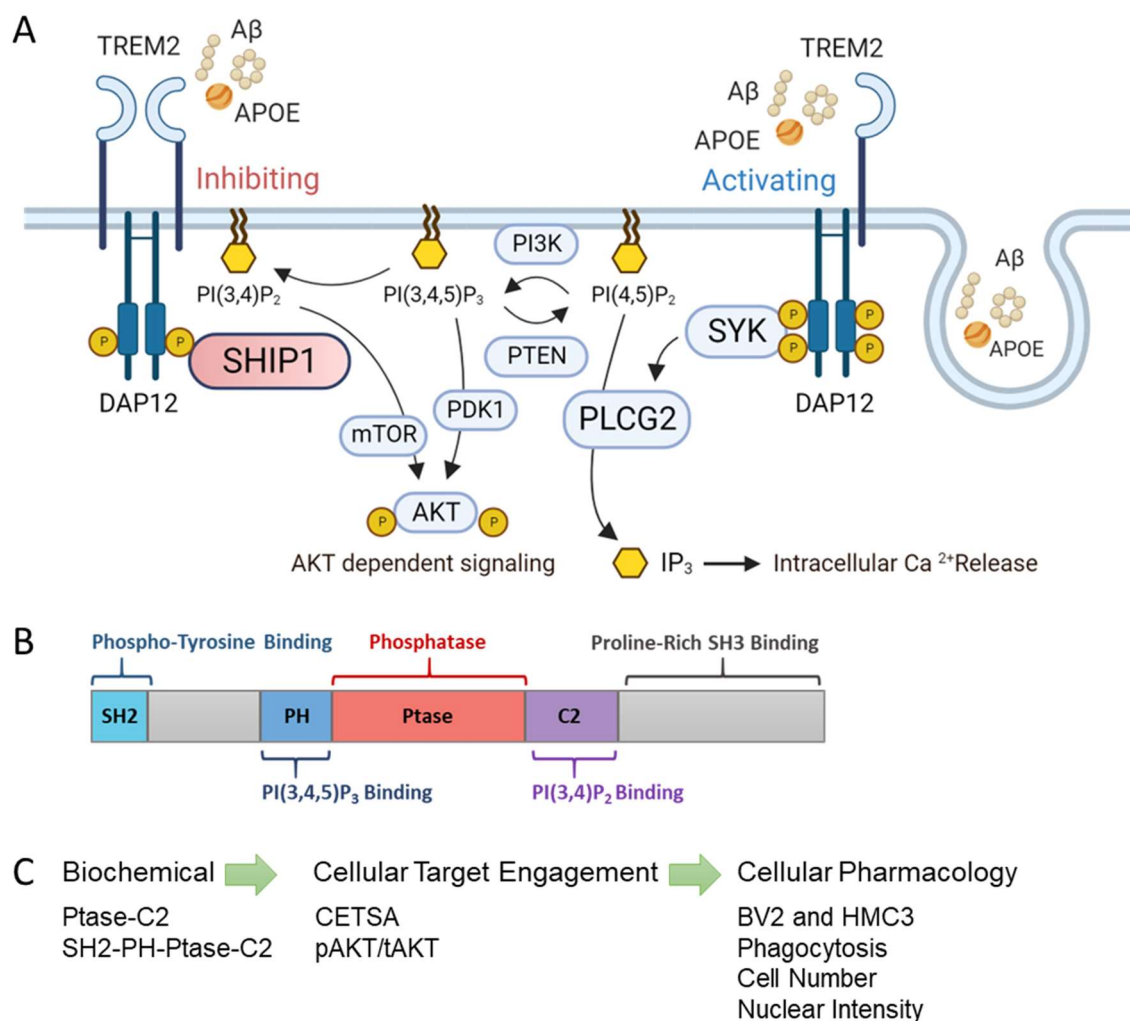


Figure 1A. TREM2 binds A β and APOE, which activate microgliosis and phagocytosis. DAP12 mediates TREM2 activation through SYK and PLC γ 2. SHIP1 completes with SYK and modulates PIP3-dependent PLC γ 2 and AKT signaling downstream from TREM2 by converting PI(3,4,5)P₃ to PI(3,4)P₂, both of which can activate AKT through PDK- and mTor-dependent mechanisms depending on cell context. **Figure 1B.** Multi-domain structure of SHIP1 containing an N-terminal SH2 that binds ITIMs and ITAMs, a phosphatase (Ptase) domain flanked by a PH domain that binds PI(3,4,5)P₃ and a C2 domain that binds PI(3,4)P₂, and a disordered C-terminal end that binds many other proteins. **Figure 1C.** Flow of assays developed to assess SHIP1 inhibitors. The development of a cellular thermal shift assay (CETSA) to ensure cellular target engagement and a phenotypic assay with simultaneous measures of microglia activation (phagocytosis) and health (cell number and nuclear intensity) were critical for identifying compounds that engaged SHIP1 and resulted in desired pharmacology.

Purdue TREAT-AD Center is reporting a chemical probe TEP with methods and experimental tools that we hope will catalyze and support further investigation into SHIP1 as a target for the treatment of AD⁶.

The inositol polyphosphate-5-phosphatase (*INPP5D*) gene has been identified as a risk gene for AD by a meta-analysis of four large genome-wide association studies (GWAS)⁷ and has been nominated as a therapeutic target by three teams within the Accelerating Medicines Partnership for AD (AMP-AD)⁸. *INPP5D* deficiency has been shown to attenuate amyloid pathology in the 5xFAD mouse model of Alzheimer's disease⁹. *INPP5D* encodes the Src homology 2 (SH2) domain-containing inositol polyphosphate 5-phosphatase 1 (SHIP1), a phosphatidylinositol phosphatase that regulates pathways downstream from TREM2^{10,11} and the Fcγ receptor FCγRIIB^{11,12}.

Triggering Receptor Expressed On Myeloid Cells 2 (TREM2) is a cell surface receptor expressed on immune cells. TREM2 plays a crucial role modulating microglial response to neurotoxins and inflammation in the brain (**Figure 1A**). Hypomorphic variants of TREM2 have been associated with an increased risk of developing AD, and researchers have been exploring ways to activate TREM2 to potentially influence disease progression; however, results directly modulating TREM2 vary and the data conflicting, depending on the model system used^{13,14}. SHIP1 is a negative regulator downstream from TREM2. This complex, multidomain protein possesses a phosphatase (Ptase) domain flanked by a pleckstrin-homology (PH) domain that binds phosphatidylinositol (3,4,5)-trisphosphate [PI(3,4,5)P₃] and a C2 domain that binds phosphatidylinositol (3,4)-bisphosphate [PI(3,4)P₂] (**Figure 1B**)^{15,16}. The PH and C2 locate and orient the Ptase catalytic site towards its PI(3,4,5)P₃ substrate at the intracellular side of the membrane. The C2 domain is essential for cellular function, and interactions between Ptase and C2 modulate enzymatic activity¹⁷. SHIP1 converts PI(3,4,5)P₃ to PI(3,4)P₂, which are phosphorylated phosphatidylinositols that play important roles in membrane structure and identity and mediate downstream pathways such as AKT/mTOR signaling. For example, PI(3,4,5)P₃ binds and activates the PH-containing proteins PLCγ2, PDK1, and AKT¹⁸. SHIP1 also contains an N-terminal SH2 domain that binds ITIMs and ITAMs on DAP12¹⁰ and FCγRIIB^{12,19} and a C-terminal proline-rich domain that binds many other proteins, including PLCγ2 and the Tec and Syk family kinases²⁰. Therefore, SHIP1 is also involved in protein–protein interactions that modulate membrane structure and downstream signaling. Because SHIP1 binds receptor ITIMs and ITAMs, competes with kinases, and converts PI(3,4,5)P₃ to PI(3,4)P₂, it is generally understood as negative regulator of cellular activation¹¹. Although the role of SHIP1 in limiting microglial activation is not entirely understood, we hypothesize based on our previously reported human²¹ and preclinical⁹ results that inhibiting SHIP1 will increase the protective functions of microglia and reduce the rate of disease progression and cognitive decline in AD patients. Importantly, to investigate the biological function of SHIP1 and examine the consequences of its pharmacological manipulation, rigorously validated molecular tools are essential²². Therefore, we have characterized reported inhibitors, developed assays, screened for novel inhibitors, and evaluated the systemic and central exposure of a chemical probe in mice to further advance research in this area.

2 METHODS

2.1 Ligand identification

The complex, multidomain, multifunctional nature of SHIP1, mediating multiple protein-protein interactions while serving as an interfacial enzyme at the intracellular side of the microglia membrane, motivated us to pursue multiple and orthogonal ligand identification strategies with the premise that engaging the target in multiple ways with different types of ligands would provide the array of molecular tools necessary to explore the pharmacology of SHIP1 inhibition. We screened the SHIP1 Ptase domain²³, analyzed a publicly available fragment-based screen²⁴, and completed a thorough evaluation of SHIP1 and SHIP2 inhibitors reported in the literature²⁵. Our screen using only the catalytic domain of SHIP1 was biased towards identifying orthosteric, active site inhibitors. Our analysis of the fragment-based screen²⁴

focused on compounds that bind in an allosteric site at the interface between the Ptase and C2 domains. Our literature evaluation focused on identifying starting points with drug-like properties and the synthesis of analogs to explore their potential for brain penetration. In each case, we prioritized chemical scaffolds that showed evidence of target engagement in cellular and *in vivo* biological contexts with the expectation that ligands that engage the target differently would have different pharmacological activities depending on the biological context, timing, and the endpoints being evaluated.

2.2 *in vitro* Assay development

Once compounds were identified, they were evaluated in a series of SHIP1-related assays (**Figure 1C**). Due to the multidomain and multifunctional nature of SHIP1, we anticipated that discrepancies may arise between enzyme and cell assays, which could subsequently confound the interpretation of cellular results, as has been previously reported^{26,27}. However, since enzyme activity is easily measured and provides evidence of target engagement, we elected to use the malachite green assay using PtdIns(3,4,5)P₃-diC8 as a substrate and a minimal enzyme construct containing the Ptase-C2 domains. This assay is standard in the field and is amenable to automated high-throughput screening^{28,29}. The Ptase-C2 protein is well behaved, can be expressed and purified to a high degree of purity, and contains the allosteric site at the interface between the Ptase and C2 domains. For comparison and to assess potential species differences, inhibitors were tested against nearly full-length and stable SHIP1 protein constructs containing all ordered domains of the human and mouse proteins. We used a SHIP1 cellular thermal shift assay (CETSA) to provide evidence of target engagement in cellular assays. Since THP1 cells are frequently employed as a model of monocyte cells and SHIP1-dependent AKT signaling has been previously observed in this cellular context^{30,31}, a signaling assay was established using THP1 cells measuring total AKT (tAKT) and phospho-Akt (pAKT) levels, which provides further evidence of on-target pharmacology. A phenotypic high-content imaging assay with simultaneous measures of phagocytosis, cell number, and nuclear intensity was used to ensure the compounds are affecting desired cellular pharmacology without cytotoxicity³². Model cell lines, BV2 and HMC3, were used to provide adequate throughput for Structure Activity Relationship (SAR) studies. Primary mouse microglia were used to ensure observations in BV2 cells reflect primary cell activity.

2.3 *in vivo* Evaluation

To support therapeutic target validation studies of pharmacological SHIP1 inhibition *in vivo*, we selected a chemical probe with desired cellular pharmacology, analyzed its ADME properties *in silico*, assessed key physicochemical and ADMET properties *in vitro*, and utilized the results to predict plasma PK profiles. We then conducted a single-dose PK study to confirm systemic peripheral and central exposures can be obtained in mice upon oral administration.

3 RESULTS

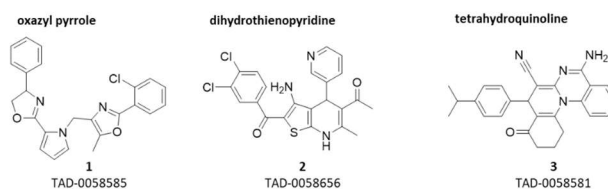
3.1 SHIP1 inhibitors

As described in our Screening Target Enablement Resource²³, 95K compounds were screened at 10 μ M using the SHIP1 Ptase domain and produced three chemical series that were selected for further study (**Figure 2A**). The oxazyl pyrrole scaffold is represented by TAD-0058585 (**1**), the dihydrothienopyridine scaffold is represented by TAD-0058656 (**2**), and the tetrahydroquinoline scaffold is represented by TAD-0058581 (**3**).

Because this screen was run using only the catalytic domain of SHIP1, these inhibitors are assumed to be orthosteric. Further elaboration and characterization of these scaffolds will be described elsewhere. Our analysis of the fragment-based, X-ray crystallography screen focused on reported compounds **4** (x-0524) and **8** (x-0101), which showed interpretable electron density in a binding pocket (Site 3) near Cys505 in the interface between the Ptase and C2 domains (**Figure 2B**). Studies with SHIP2 have demonstrated that the C2 domain is essential for cellular function, and its rigid interface with the Ptase domain enhances enzymatic activity¹⁷. Because the reported fragments did not inhibit SHIP1, we prepared analogs with improved activity. Adding a cyano group (**5**, **6**) to x-0524 proved effective, demonstrating increasing potency in the enzyme assay. The addition of 4-methyl benzoate (**7**) also improved enzyme inhibitory activity. Since this binding site contains a potentially reactive cysteine, we added the reactive functional group acryloyl to x-0101 to give compound **9**, which inhibited the enzyme, was active in CETSA, and yielded a crystal structure of the covalently modified protein (to be deposited in the Protein Data Bank (PDB)). This structure is overlaid with the cocrystal structure of x-0101 and SHIP1 (PDB 5RWL)³³ in **Figure 2B**. These data provide evidence for binding in allosteric site 3 in the interface between the Ptase and C2 domains.

SHIP1 and SHIP2 inhibitors reported in the literature²⁵ are described in **Figure 3**. Metabolically stabilized analogs

A. Screening Hits



B. Fragments

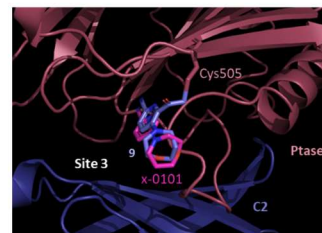
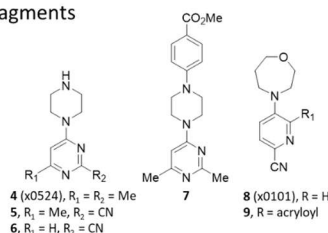


Figure 2A. SHIP1 Ptase domain inhibitors identified by high throughput screening. **Figure 2B.** Fragment-based scaffold. Fragments **4** (x0524) and **8** (x0101) did not inhibit SHIP1. Adding cyano and 4-methyl benzoate groups to x0524 (**5-7**) increased enzyme potency and cellular target engagement. Compound **9** reacted with Cys505 and provided a crystal structure (overlayed with PDB 5RWL).

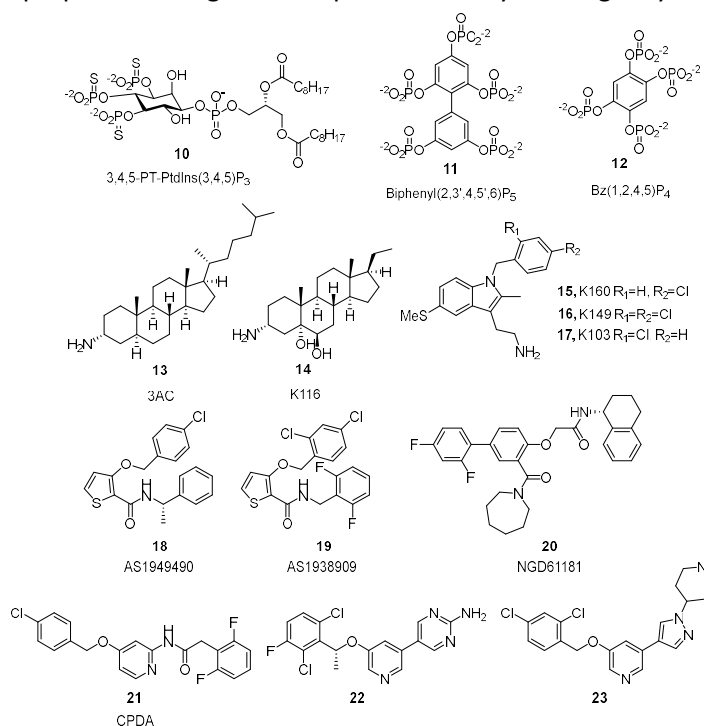


Figure 3. SHIP1 inhibitors reported in the literature.

of PtdIns(3,4,5)P₃, such as **10**, are stable, are not degraded by phosphatidylinositol phosphatases, and act as inhibitors³⁴; however, they are not selective for SHIP1 nor do they have the physicochemical properties required for studies beyond cellular assays. Likewise, phosphorylated polyphenols³⁵, such as **11** and **12**, were deemed inadequate for our purposes because they are highly charged and therefore unable to cross cell membranes. Therefore, we did not characterize these compounds. The aminosteroid **13**, known as 3 α -aminocholestane (3AC), was first reported by the Kerr group³⁶ and is the most widely used SHIP1 inhibitor^{25,36-39}. We also prepared and evaluated the more soluble aminosteroid analog K116 (**14**)^{40,41} and several analogs of a tryptamine scaffold (**15-17**) reported by the Kerr group³⁷. We obtained AS1949490 (**18**) and AS1938909 (**19**), a thiophene scaffold described by Astellas Pharma^{42,43} as a selective SHIP2 inhibitor with minimal activity against SHIP1. We also prepared NGD61181 (**20**), which was discovered by NeoGenesis Pharmaceuticals⁴⁴ using MS-based affinity screening of a combinatorial library. Researchers at the University of Toyama noted similarities between the compounds reported by Astellas and NeoGenesis and used them as a starting point for a ligand-based design effort, culminating in the synthesis and evaluation of a pyridyl-based scaffold best represented by N-[4-(4-Chlorobenzyloxy)pyridin-2-yl]-2-(2,6-difluorophenyl) acetamide (CPDA, **21**)⁴⁵. A similar pyridyl scaffold has been reported based on the observation that crizotinib, a multi-targeted kinase inhibitor, also inhibits SHIP2⁴⁶. We prepared several analogs from this report, including compounds **22** and **23**.

Preparation of compounds.

Compounds used in this study were purchased or prepared according to procedures described below. Structure activity relationship studies around hit scaffolds from our screen of the SHIP1 Ptase domain²³ and the publicly available fragment-based screen²⁴ will be detailed elsewhere.

Reagents and solvents were purchased from commercial sources and used without further purification. All reactions involving air- or moisture-sensitive reagents were performed under a nitrogen or argon atmosphere. NMR spectra were recorded on Bruker Avance Neo 400 MHz or DRX500-1 500 MHz instruments. For ¹H NMR, chemical shifts in ppm relative to the residual solvent peak, multiplicities, coupling constants in Hertz, and numbers of protons are indicated. Reactions were routinely monitored by analytical TLC and/or LC-MS. Analytical TLC was performed on silica gel 60 F₂₅₄ silica gel plates, and 254 nm UV light and/or I₂ staining were used for visualization. Reaction monitoring LC-MS data were obtained on a Waters Acquity UPLC system equipped with UV (TUV or PDA), mass (SQD2 or QDa), and/or evaporative light scattering detectors. Flash NP or RP chromatography were performed on a Teledyne-ISCO NextGen 300 instrument using prepacked silica gel or C18-functionalized silica gel columns available from Teledyne-ISCO, or on a Teledyne-ISCO Combiflash using prepacked silica gel columns available from Agela or Welch. High-resolution mass spectra were obtained on an Agilent 6550 Q-TOF instrument. All compounds had $\geq 95\%$ purity as determined by LC-MS, and one of the following specified methods was used to determine test compound purity:

LC-MS Method A: mobile phase A, 0.1% formic acid in H₂O; mobile phase B, 0.1% formic acid in ACN; column, Acquity BEH C18 (1.7 μ m, 50 mm x 2.1 mm); flow rate, 0.6 mL/min; detection wavelength, 254 nm; column temperature, 40 °C.

LC-MS Method B: mobile phase A, 0.1% TFA in H₂O; mobile phase B, ACN; column, Acquity HSS-T3 (1.8 μ m, 100 mm x 2.1 mm); flow rate, 0.3 mL/min; detection wavelength, 214 nm; column temperature, 30°C.

LC-MS Method C: Same as LC-MS Method B except detection was by ELSD. Details: gas pressure, 4 bar; drift tube temperature, 45 °C; gain, 10; noise filter, 0.5.

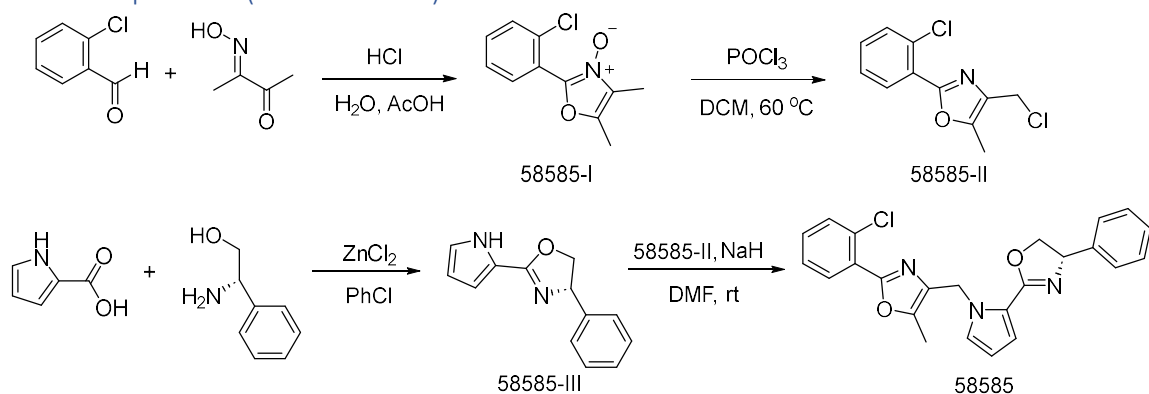
LC-MS Method D: mobile phase A, 5 mM NH₄OAc in H₂O; mobile phase B, ACN; column, Acquity BEH C18 (1.7 μ m, 100 mm x 2.1 mm); flow rate, 0.3 mL/min; detection wavelength, 214 nm; column temperature, 30 °C.

LC-MS Method E: mobile phase A, 0.1% TFA in H₂O; mobile phase B, MeOH; column, Acquity HSS-T3 (1.8 μ m, 100 mm x 2.1 mm); flow rate, 0.3 mL/min; detection wavelength, 214 nm; column temperature, 30 °C.

LC-MS Method F: mobile phase A, 5 mM NH₄OAc in H₂O; mobile phase B, ACN; column, Acquity BEH C18 (1.7 μ m, 100 mm x 2.1 mm); flow rate, 0.3 mL/min; detection wavelength, 214 nm; column temperature, 30 °C.

LC-MS Method G: mobile phase A, 0.1% TFA in H₂O; mobile phase B, ACN; column, Acquity HSS-T3 (1.8 μ m, 100 mm x 2.1 mm); flow rate, 0.3 mL/min; detection wavelength, 214 nm; column temperature, 30 °C.

Synthesis of Compound 1 (TAD-0058585)



2-(2-Chlorophenyl)-4,5-dimethyloxazole 3-oxide (58585-I). A mixture of 2,3-butanedione monoxime (0.90 g, 8.90 mmol) and 2-chlorobenzaldehyde (1.37 g, 9.79 mmol, 1.1 equiv.) in acetic acid (50 mL) was cooled to 0 °C and a solution of HCl (4.0 M in dioxane, 3.4 mL, 1.5 equiv.) was added. The reaction mixture was allowed to warm to room temperature and stirred for 16 h, diluted with methyl tert-butyl ether and filtered. The solid was collected, washed with ethyl ether, and dried to afford the oxazole oxide product as a white solid (1.42 g, 6.35 mmol, 71% yield), which was used without further purification.

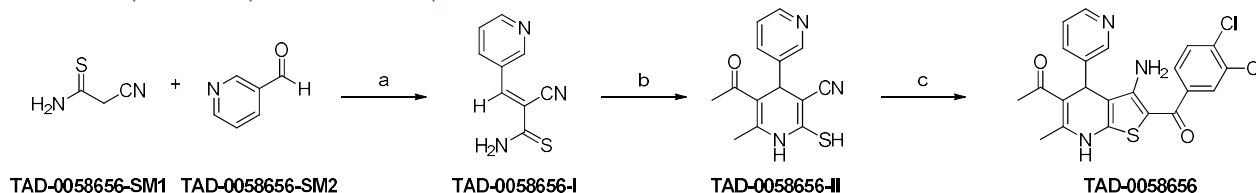
4-(Chloromethyl)-5-methyl-2-(2-chlorophenyl)oxazole (58585-II). To a solution of 2-(2-Chlorophenyl)-4,5-dimethyloxazole 3-oxide (1.12 g, 4.47 mmol) in DCE (30 mL), was added POCl₃ (460 μ L, 4.92 mmol, 1.1 equiv.). The reaction was heated at reflux for 30 min, then cooled to rt, carefully quenched with water, and extracted with DCM (2 x 20 mL). The evaporated residue was purified by silica gel chromatography (0~40% EtOAc in hexanes) to afford the chloromethyloxazole product as a colorless oil (0.64 g, 2.64 mmol, 53% yield). ¹H NMR (500 MHz, CDCl₃) δ 7.98–7.92 (m, 1H), 7.48–7.44 (m, 1H), 7.37–7.30 (m, 2H), 4.58 (s, 2H), 2.44 (s, 3H). LC/MS m/z calculated [M+H]⁺. 242.01, found 242.10.

(4S)-5-methyl-4-phenyl-2-(1H-pyrrol-2-yl)-4,5-dihydrooxazole (58585-III). ZnCl₂ (68 mg, 0.5 mmol, 0.05 eq.) was melted in vacuo and then cooled under N₂. Chlorobenzene (30 mL), L-phenylglycinol (1.37g, 10 mmol) and 2-pyrrole-carbonitrile (0.92 g, 10 mmol) were added. After refluxing for 24 h, the solvent was evaporated, and the resulting mixture was purified by silica gel chromatography (40~80% EtOAc in hexanes) to yield the product as a white powder (0.51 g, 2.40 mmol, 24% yield). ¹H NMR (500 MHz, CDCl₃) δ 10.77 (br s, 1H), 7.40–7.24 (m, 5H), 6.77 (dd, *J* = 3.6, 1.5 Hz, 1H), 6.26 (dd, *J* = 2.6, 1.5 Hz, 1H), 6.13 (dd, *J* = 3.6, 2.6 Hz, 1H), 5.31 (dd, *J* = 9.7, 7.6 Hz, 1H), 4.72 (dd, *J* = 9.8, 8.2 Hz, 1H), 4.22 (dd, *J* = 8.2, 7.6 Hz, 1H). LC/MS m/z calculated [M+H]⁺. 227.12, found 227.20.

2-(2-chlorophenyl)-5-methyl-4-((2-((4S)-5-methyl-4-phenyl-4,5-dihydrooxazol-2-yl)-1H-pyrrol-1-yl)methyl)oxazole (TAD-0058585). To a solution of 3 (0.43g, 2 mmol) in DMF was added NaH (2 eq.) at 0 °C, and the solution was stirred for 30min. Then a solution of 2 was added dropwise to the mixture at

0 °C. The resulting mixture was warmed to rt and stirred for 4h. The reaction was then quenched with water (10 mL), and extracted with EtOAc, and the combined organic layer was washed with water and brine. The evaporated residue was purified by silica gel chromatography (30~60% EtOAc in hexanes) to afford the product as a light-yellow solid. ¹H NMR (500 MHz, CDCl₃) δ 7.93 – 7.88 (m, 1H), 7.50 – 7.44 (m, 1H), 7.36 – 7.27 (m, 7H), 7.20 (dd, *J* = 2.7, 1.8 Hz, 1H), 6.99 (br s, 1H), 6.26 – 6.21 (m, 1H), 5.70 (q, *J* = 15.2 Hz, 2H), 5.40 (dd, *J* = 9.9, 7.7 Hz, 1H), 4.74 – 4.67 (m, 1H), 4.22 – 4.16 (m, 1H), 2.20 (s, 3H). ¹³C NMR (126 MHz, CDCl₃) δ 159.16, 157.72, 146.64, 142.29, 132.74, 132.29, 131.10, 130.77, 128.75, 127.68, 126.76, 126.70, 126.48, 116.58, 108.86, 73.71, 69.61, 43.72, 10.15. LC/MS *m/z* calculated [M+H]⁺. 432.15, found 432.20.

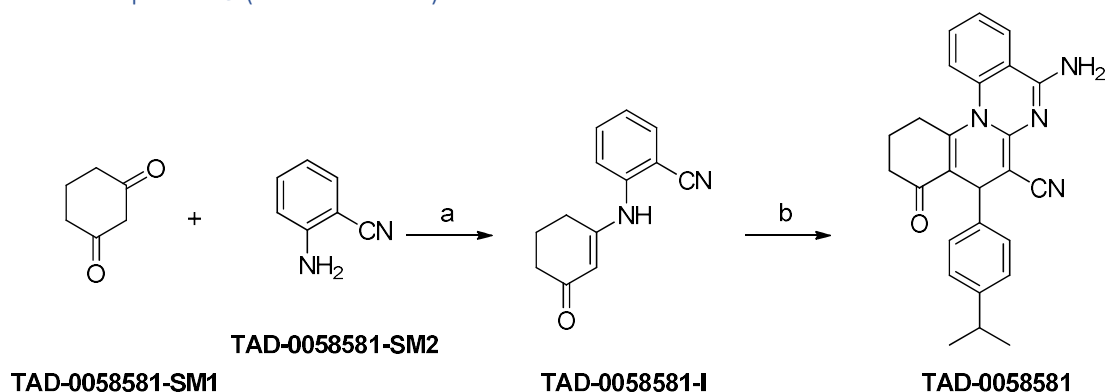
Synthesis of Compound 2 (TAD-0058656)



Reaction conditions: (a) piperidine, ethanol, r.t., 0.5 h; (b) 3,5-heptanedione, piperidine, r.t., 1 h; then 60°C, 2 h; (c) 3,4-dichlorophenacyl bromide, K₂CO₃, r.t., overnight.

Synthesis of 1-(3-amino-2-(3,4-dichlorobenzoyl)-6-methyl-4-(pyridin-3-yl)-4,7-dihydrothieno[2,3-b]pyridin-5-yl)ethanone (TAD-0058656). 2-Cyanothioacetamide (2.0 g, 20 mmol), 3-pyridinecarboxaldehyde (2.14 g, 20 mmol), and piperidine (0.2 ml, 2 mmol) are dissolved in ethanol (40 ml). The mixture is stirred at ambient temperature for half an hour. Then 3,5-heptanedione (2.7 ml, 20 mmol) is added dropwise to the reaction mixture followed by an additional portion of piperidine (2.4 ml, 24 mmol). The reaction is stirred at ambient temperature for 1 hour then heated in a 60 °C heating bath for 2 hours. The reaction is cooled in a water-ice bath. 3,4-dichlorophenacyl bromide (5.36 g, 20 mmol) and potassium carbonate (5.52 g, 40 mmol) are added to the reaction in sequence. The reaction is removed from the cooling bath and stirred overnight at ambient temperature. The crude reaction is diluted with water and washed with ethyl acetate. The organic extract is dried over sodium sulfate. Solvents are removed by rotary evaporator and the residue purified by flash chromatography (silica gel, ethyl acetate : hexane =1:1) to obtained the product, 1-(3-amino-2-(3,4-dichlorobenzoyl)-6-methyl-4-(pyridin-3-yl)-4,7-dihydrothieno[2,3-b]pyridin-5-yl)ethanone, as a yellow solid (4.5 g, 49.2% yield). ¹H NMR (500 MHz, DMSO) δ 10.20 (s, 1H), 8.60 (d, *J* = 2.0 Hz, 1H), 8.35 (dd, *J* = 4.7, 1.6 Hz, 1H), 7.82 (d, *J* = 2.0 Hz, 1H), 7.73 (d, *J* = 8.3 Hz, 1H), 7.68 – 7.65 (m, 1H), 7.58 (dd, *J* = 8.3, 2.0 Hz, 1H), 7.29 (dd, *J* = 7.7, 4.7 Hz, 1H), 5.31 (s, 1H), 2.35 (s, 3H), 2.18 (s, 3H). ¹³C NMR (126 MHz, DMSO) δ 196.07, 181.77, 155.59, 148.50, 147.65, 146.73, 146.24, 141.57, 141.16, 134.81, 132.99, 131.26, 130.79, 129.06, 127.28, 123.77, 110.61, 110.54, 98.73, 35.23, 30.43, 20.16. LC/MS *m/z* calculated [M+H]⁺. 458.05, found 458.10.

Synthesis of Compound 3 (TAD-0058581)

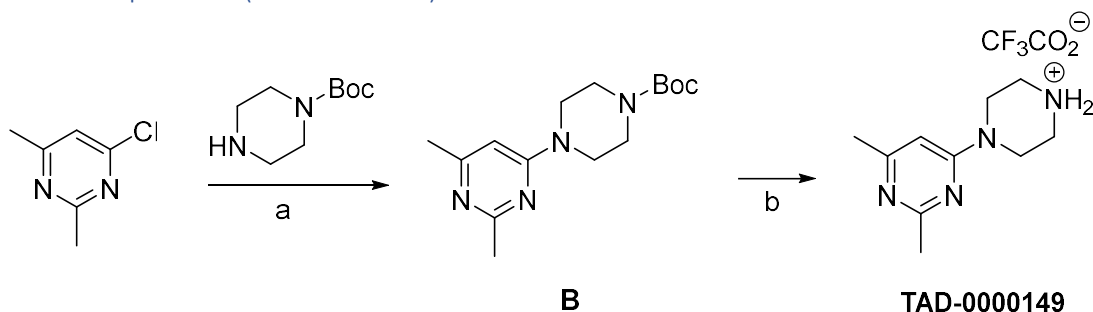


Reaction conditions: (a) I₂, acetonitrile, r.t., overnight; (b) 4-isopropylbenzaldehyde, ethylene glycol, malononitrile, 120°C, 16 h.

Synthesis of 2-((3-oxocyclohex-1-en-1-yl)amino)benzonitrile (TAD-0058581-I). A mixture of 2-aminobenzonitrile (5.0 g, 42.32 mmol), cyclohexane-1,3-dione (4.75 g, 42.32 mmol), and iodine (0.22 g, 0.85 mmol) was taken in a round-bottomed flask in 100 ml of acetonitrile and stirred at room temperature overnight. After completion of the reaction, EtOAc (100mL) was added, and the mixture washed with hot water (100 mL) followed by 0.2 M HCl aq (100 mL) and dried over MgSO₄. Solvents are removed by rotary evaporator and the residue purified by flash chromatography (silica gel, ethyl acetate : hexane =3:1) to obtained the product, as a brown solid (7.1 g, 79% yield). LC/MS m/z calculated [M+H]⁺. 213.10, found 213.20.

Synthesis of 5-amino-8-(4-isopropylphenyl)-9-oxo-9,10,11,12-tetrahydro-8H-quinolino[1,2-a]quinazoline-7-carbonitrile (TAD-0058581). A mixture containing 4-isopropylbenzaldehyde (70 mg, 0.47 mmol), malononitrile (32 mg, 0.47 mmol), 2-((3-oxocyclohex-1-en-1-yl)amino)benzonitrile (100 mg, 0.47 mmol) and ethylene glycol (3.0 mL) was introduced into a 10 mL reaction vial, the vial was capped and the mixture was then stirred at 120 °C (oil bath temperature) for 16 hours. When the reaction was completed (TLC monitoring), the reaction mixture was cooled to room temperature and then poured into cold water. The solid product was filtered, washed with water and EtOH (95%), and subsequently dried and purified by flash chromatography (silica gel, ethyl acetate : hexane =1:3) to obtained the product, and further recrystallized from EtOH (95%) to give the pure product as a yellow solid (87 mg, 45% yield). ¹H NMR (500 MHz, DMSO) δ 8.04 (s, 2H), 7.96 (d, *J* = 7.1 Hz, 1H), 7.61 (t, *J* = 7.3 Hz, 1H), 7.43 (d, *J* = 8.3 Hz, 1H), 7.33 (t, *J* = 7.6 Hz, 1H), 7.07 (q, *J* = 8.4 Hz, 4H), 4.57 (s, 1H), 3.47 – 3.41 (m, 1H), 2.76 (dt, *J* = 13.8, 6.9 Hz, 1H), 2.58 – 2.51 (m, 1H), 2.40 (dt, *J* = 8.9, 4.2 Hz, 1H), 2.32 (dd, *J* = 9.7, 6.1 Hz, 1H), 2.06 (dt, *J* = 12.9, 4.5 Hz, 1H), 1.93 (dd, *J* = 23.4, 11.7 Hz, 1H), 1.11 (s, 3H), 1.08 (s, 3H). ¹³C NMR (126 MHz, DMSO) δ 195.48, 156.17, 152.95, 152.85, 146.71, 140.71, 137.29, 132.81, 126.52, 126.19, 124.84, 124.31, 121.29, 120.51, 119.67, 115.60, 73.89, 36.97, 36.23, 32.98, 28.23, 23.85, 23.80, 23.71. LC/MS m/z calculated [M+H]⁺. 409.20, found 409.20.

Synthesis of Compound 4 (TAD-0000149).

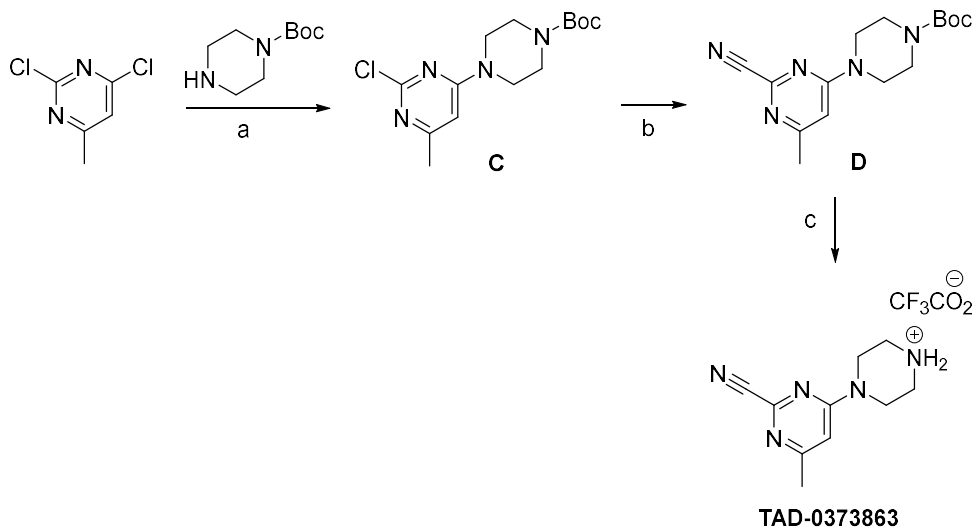


Reagents and conditions: (a) DIPEA, iPrOH, 110°C, 16h; (b) TFA, DCM, 0°C to rt, 3h.

Tert-butyl 4-(2,6-dimethylpyrimidin-4-yl)piperazine-1-carboxylate (B). To a solution of 4-chloro-2,6-dimethylpyrimidine (500 mg, 3.51 mmol, 1 eq) in iPrOH (5 mL) was added DIPEA (1.362 g, 10.54 mmol, 3 eq) and 1-Boc-piperazine (327 mg, 1.76 mmol, 0.5 eq). The reaction mixture was heated to 110°C for 16h. The reaction mixture was then diluted with cold H₂O and extracted with EtOAc. The combined organic extracts were dried over Na₂SO₄, filtered, and concentrated. The residue was purified by flash LC on silica gel, eluting with 50:50 hexanes:EtOAc, to provide intermediate **B** (480 mg, 47%) as an oil. ¹H NMR (400 MHz, DMSO-*d*₆) δ 6.50 (s, 1H), 3.65 – 3.50 (m, 4H), 3.45 – 3.35 (m, 4H), 2.32 (s, 3H), 2.22 (s, 3H), 1.42 (s, 9H); LRMS (ES⁺) *m/z* 293.02 [M+H]⁺.

4-(2,6-Dimethylpyrimidin-4-yl)piperazin-1-ium 2,2,2-trifluoroacetate [TAD-0000149 or x0524]. To a solution of intermediate **B** (300 mg, 1.03 mmol, 1 eq) in DCM (5 mL) at 0°C was added TFA (585 mg, 5.13 mmol, 5 eq). The reaction mixture was stirred with warming to rt for 3h. The reaction mixture was concentrated and triturated with pentane to provide the title product (150 mg, 48%) as a white solid. ¹H NMR (400 MHz, DMSO-*d*₆) δ 9.07 (s, 2H), 7.07 (s, 1H), 4.15 – 3.85 (m, 4H), 3.30 – 3.20 (m, 4H), 2.53 (s, 3H), 2.41 (s, 3H); LRMS (ES⁺) *m/z* 193.11 [M+H]⁺; LC-MS purity 99.75% (LC-MS Method E).

Synthesis of Compound 5 (TAD-0373863).



Reagents and conditions: (a) DIPEA, iPrOH, 100°C, 16h; (b) Zn(CN)₂, Zn, dppf, Pd₂dba₃, DMF, 100°C, 16h; (c) TFA, DCM, 0°C to rt, 2h.

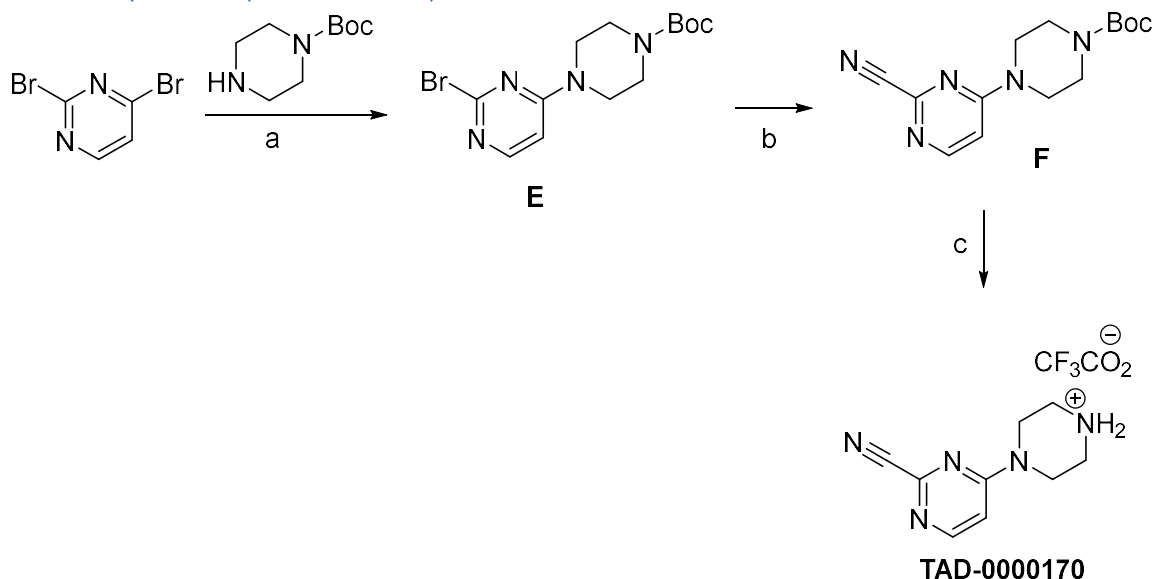
Tert-butyl 4-(2-chloro-6-methylpyrimidin-4-yl)piperazine-1-carboxylate (C). To a stirring solution of 2,4-dichloro-6-methylpyrimidine (1.00 g, 6.13 mmol, 1 eq) and 1-Boc-piperazine (1.25 g, 6.71 mmol, 1.1 eq) in iPrOH (10 mL) was added DIPEA (3.2 mL, 18 mmol, 3 eq). The reaction mixture was

stirred at 100°C for 16h. The reaction mixture was concentrated. The residue was purified by flash LC on silica gel, eluting with 70:30 hexanes:EtOAc, to provide intermediate **C** (1.00 g, 52%) as a light brown solid. ¹H NMR (400 MHz, DMSO-*d*₆) δ 6.73 (s, 1H), 3.70 – 3.50 (m, 4H), 3.50 – 3.35 (m, 4H), 2.25 (s, 3H), 1.42 (s, 9H); LRMS (ES⁺) *m/z* 313.11 [M+H]⁺.

Tert-butyl 4-(2-cyano-6-methylpyrimidin-4-yl)piperazine-1-carboxylate (D). To a stirred solution of intermediate **C** (500 mg, 1.60 mmol, 1 eq) in DMF (5 mL) was added Zn(CN)₂ (282 mg, 2.40 mmol, 1.5 eq) and Zn (26.1 mg, 0.399 mmol, 0.25 eq). The reaction mixture was purged with Ar for 20 min, then dppf (88.6 mg, 0.160 mmol, 0.1 eq) and Pd₂dba₃ (146 mg, 0.160 mmol, 0.1 eq) were added and the reaction mixture was stirred at 100°C for 16h. The reaction mixture was diluted with chilled H₂O and extracted with EtOAc. The combined organic extracts were washed with H₂O, then with brine, dried over Na₂SO₄, filtered, and concentrated. The residue was purified by flash LC on silica gel, eluting with 100:0 to 40:60 hexanes:EtOAc, to provide intermediate **D** (300 mg, 62%) as an off-white solid. ¹H NMR (400 MHz, DMSO-*d*₆) δ 7.01 (s, 1H), 3.70 – 3.55 (m, 4H), 3.45 – 3.35 (m, 4H), 2.31 (s, 3H), 1.42 (s, 9H); LRMS (ES⁺) *m/z* 304.15 [M+H]⁺.

4-(2-Cyano-6-methylpyrimidin-4-yl)piperazin-1-ium 2,2,2-trifluoroacetate [TAD-0373863]. To a stirring solution of intermediate **D** (150 mg, 0.494 mmol, 1 eq) in DCM (5 mL) at 0°C was added TFA (2 mL). The reaction mixture was stirred at rt for 2h. The reaction mixture was concentrated. The residue was triturated with Et₂O to provide the title product (0.060 g, 38%) as a brown solid. ¹H NMR (400 MHz, DMSO-*d*₆) δ 8.87 (s, 2H), 7.11 (s, 1H), 3.90 – 3.80 (m, 4H), 3.25 – 3.15 (m, 4H), 2.34 (s, 3H); LRMS (ES⁺) *m/z* 204.18 [M+H]⁺; LC-MS purity 98.85% (LC-MS Method F).

Synthesis of Compound **6** (TAD-0000170).



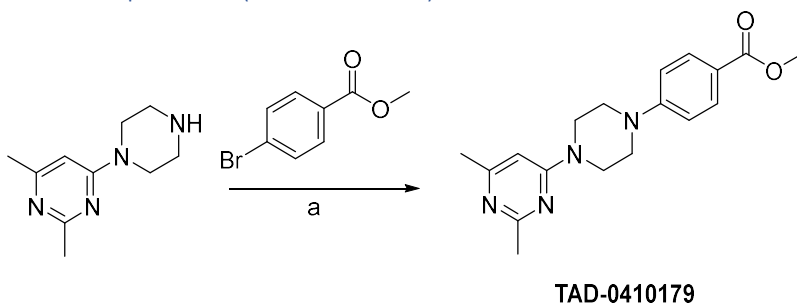
Reagents and conditions: (a) DIPEA, iPrOH, 100°C, 16h; (b) Pd₂(dba)₃, dppf, Zn(CN)₂, DMF, 110°C, 16h; (c) TFA, DCM, 0°C, 2h.

Tert-butyl 4-(2-bromopyrimidin-4-yl)piperazine-1-carboxylate (E). To a stirring solution of 2,4-dibromopyrimidine (300 mg, 1.26 mmol, 1 eq) and 1-Boc-piperazine (235 mg, 1.26 mmol, 1 eq) in iPrOH (5 mL) was added DIPEA (0.7 mL, 4 mmol, 3 eq). The reaction mixture was stirred at 100°C for 16h. The reaction mixture was concentrated. The residue was purified by flash LC on silica gel, eluting with hexanes:EtOAc, to provide intermediate **E** (220 mg, 51%) as a brown solid. LRMS (ES⁺) *m/z* 345.24 [M+H]⁺.

Tert-butyl 4-(2-cyanopyrimidin-4-yl)piperazine-1-carboxylate (F). A stirring solution of intermediate E (220 mg, 0.641 mmol, 1 eq) and $\text{Zn}(\text{CN})_2$ (153 mg, 1.30 mmol, 2 eq) in DMF (5 mL) was purged with N_2 for 10 min. Then $\text{Pd}_2(\text{dba})_3$ (58 mg, 0.063 mmol, 0.1 eq) and dppf (35 mg, 0.063 mmol, 0.1 eq) were added. The reaction mixture was stirred at 110°C for 16 h. The reaction mixture was concentrated. The residue was purified by flash LC on silica gel, eluting with hexanes:EtOAc, to provide intermediate F (170 mg, 92%) as a brown solid. ^1H NMR (400 MHz, $\text{DMSO}-d_6$) δ 8.29 (d, $J = 6.4$ Hz, 1H), 7.10 (d, $J = 6.4$ Hz, 1H), 3.75 – 3.55 (m, 4H), 3.50 – 3.35 (m, 4H), 1.42 (s, 9H); LRMS (ES^+) m/z 290.29 $[\text{M}+\text{H}]^+$.

4-(2-Cyanopyrimidin-4-yl)piperazin-1-ium 2,2,2-trifluoroacetate [TAD-0000170]. To a stirring solution of intermediate F (170 mg, 0.588 mmol, 1 eq) in DCM at 0°C was added TFA (0.17 mL, 2.2 mmol, 4 eq) dropwise. The reaction mixture was stirred at 0°C for 2 h. The reaction mixture was concentrated. The residue was co-evaporated with Et_2O and then triturated with Et_2O and pentane to provide the title product (20 mg, 11%) as a brown solid. ^1H NMR (400 MHz, $\text{DMSO}-d_6$) δ 8.88 (s, 2H), 8.38 (d, $J = 6.4$ Hz, 1H), 7.19 (d, $J = 6.4$ Hz, 1H), 3.95 – 3.80 (m, 4H), 3.30 – 3.15 (m, 4H); LRMS (ES^+) m/z 190.15 $[\text{M}+\text{H}]^+$; LC-MS purity 95.88% (LC-MS Method G).

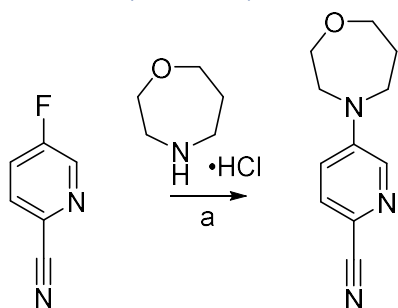
Synthesis of Compound 7 (TAD-0410179).



Reagents and conditions: (a) Cs_2CO_3 , Xantphos, $\text{Pd}_2(\text{dba})_3$, 100°C , 16h.

Methyl 4-(4-(2,6-dimethylpyrimidin-4-yl)piperazin-1-yl)benzoate [TAD-0410179]. To a stirred solution of 2,4-dimethyl-6-(piperazin-1-yl)pyrimidine (500 mg, 2.60 mmol, 1 eq) in PhMe (5 mL) was added methyl 4-bromobenzoate (559 mg, 2.60 mmol, 1 eq) followed by Cs_2CO_3 (2.54 g, 7.80 mmol, 3 eq) and the reaction mixture was purged with Ar for 20 min. Xantphos (150 mg, 0.259 mmol, 0.1 eq) and $\text{Pd}_2(\text{dba})_3$ (238 mg, 0.260 mmol, 0.1 eq) were added and reaction mixture was heated at 100°C and stirred for 16h. The reaction mixture was diluted with H_2O and extracted with EtOAc. The combined organic extracts were washed with brine, dried over Na_2SO_4 , filtered, and concentrated. The residue was purified by flash LC on silica gel, eluting with 70:30 hexanes:EtOAc, to provide the title product (180 mg, 21%) as a white solid. ^1H NMR (400 MHz, $\text{DMSO}-d_6$) δ 7.81 (d, $J = 8.8$ Hz, 2H), 7.00 (d, $J = 9.2$ Hz, 2H), 6.55 (s, 1H), 3.78 (s, 3H), 3.75 – 3.70 (m, 4H), 3.50 – 3.40 (m, 4H), 2.35 (s, 3H), 2.23 (s, 3H); LRMS (ES^+) m/z 327.08 $[\text{M}+\text{H}]^+$; LC-MS purity 97.07% (LC-MS Method B).

Synthesis of Compound 8 (TAD-0000111).

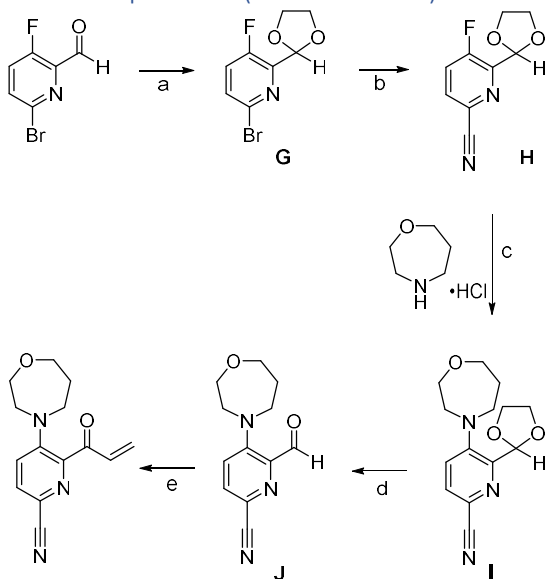


TAD-0000111

Reagents and conditions: (a) NEt_3 , ACN, reflux, overnight.

5-(1,4-Oxazepan-4-yl)picolinonitrile [TAD-0000111 or x-0101]. A mixture of 5-fluoropicolinonitrile (203 mg, 1.66 mmol, 1 eq), 1,4-oxazepane HCl (276 mg, 2.01 mmol, 1.2 eq), and NEt_3 (383 mg, 3.78 mmol, 2.3 eq) in MeCN (5 mL) was stirred at reflux overnight. The mixture was concentrated in vacuo and the residue was purified by flash LC on silica gel, eluting with 80:20 to 0:100 hexanes:EtOAc, to provide the title product (275 mg, 82%) as a white solid. ^1H NMR (500 MHz, $\text{DMSO}-d_6$) δ 8.27 (d, $J = 3.1$ Hz, 1H), 7.68 (d, $J = 8.9$ Hz, 1H), 7.21 (dd, $J = 8.9, 3.1$ Hz, 1H), 3.75 – 3.64 (m, 6H), 3.59 (t, $J = 5.4$ Hz, 2H), 1.87 (p, $J = 5.6$ Hz, 2H); LRMS (ES^+) m/z 204.2 $[\text{M}+\text{H}]^+$; HRMS (QTOF) m/z calcd for $\text{C}_{11}\text{H}_{14}\text{N}_3\text{O}$ $[\text{M}+\text{H}]^+$ 204.1131, found 204.1132; LC-MS purity 99.03% (LC-MS Method B).

Synthesis of Compound 9 (TAD-0058547).



TAD-0058547

Reagents and conditions: (a) ethylene glycol, $\text{PTSA}\cdot\text{H}_2\text{O}$, PhMe, reflux, overnight; (b) Cu(I)CN , DMF, 115°C , overnight; (c) NEt_3 , ACN, reflux, overnight; (d) TFA, DCM, reflux, 5 h; (e) i. vinylMgBr , THF, -78°C to rt, 2 h; ii. DMP, DCM, rt, 1 h.

6-Bromo-2-(1,3-dioxolan-2-yl)-3-fluoropyridine (G). A mixture of 6-bromo-3-fluoropicolinaldehyde (4.91 g, 24.1 mmol, 1 eq), ethylene glycol (2.7 mL, 48 mmol, 2 eq), and $\text{pTSA}\cdot\text{H}_2\text{O}$ (222 mg, 1.17 mmol, 0.05 eq) in PhMe (50 mL) was stirred and heated to reflux overnight, with the H_2O collected in a Dean-Stark trap. The mixture was concentrated in vacuo and the residue was purified by flash LC on silica gel, eluting with 100:0 to 80:20 hexanes:EtOAc, to provide intermediate **G** (5.76 g, 96%)

as a white solid. ^1H NMR (500 MHz, DMSO- d_6) δ 7.83 – 7.74 (m, 2H), 5.96 (s, 1H), 4.17 – 4.07 (m, 2H), 4.05 – 3.95 (m, 2H); HRMS (QTOF) m/z calcd for $\text{C}_8\text{H}_8\text{BrFNO}_2$ $[\text{M}+\text{H}]^+$ 247.9717/249.9697, found 247.9716/249.9696.

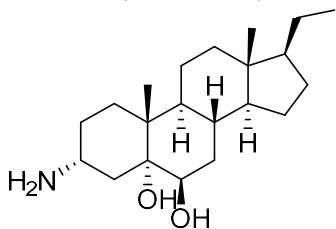
6-(1,3-Dioxolan-2-yl)-5-fluoropicolinonitrile (H). A mixture of intermediate **G** (5.50 g, 22.2 mmol, 1 eq) and Cu(I)CN (1.99 g, 22.2 mmol, 1 eq) in DMF (55 mL) was stirred at 115 °C overnight. EtOAc (55 mL) was added and the mixture was filtered through a Celite pad. The pad was washed with EtOAc (2 x 55 mL). The combined filtrate was concentrated in vacuo and the residue was purified by flash LC on silica gel, eluting with 80:20 to 40:60 hexanes:EtOAc, to provide intermediate **H** (3.37 g, 78%) as a faint yellow oil. ^1H NMR (500 MHz, DMSO- d_6) δ 8.24 (dd, J = 8.6, 3.7 Hz, 1H), 8.08 (dd, J = 10.0, 8.6 Hz, 1H), 6.04 (s, 1H), 4.18 – 4.08 (m, 2H), 4.08 – 3.98 (m, 2H); HRMS (QTOF) m/z calcd for $\text{C}_9\text{H}_8\text{FN}_2\text{O}_2$ $[\text{M}+\text{H}]^+$ 195.0564, found 195.0565.

6-(1,3-Dioxolan-2-yl)-5-(1,4-oxazepan-4-yl)picolinonitrile (I). A mixture of intermediate **H** (2.25 g, 11.6 mmol, 1 eq), 1,4-oxazepane HCl (**4**, 1.93 g, 14.0 mmol, 1.2 eq), and NEt_3 (2.72 g, 26.9 mmol, 2.3 eq) in ACN (30 mL) was stirred and heated to reflux overnight. The mixture was concentrated in vacuo and the residue was purified by flash LC on silica gel, eluting with 60:40 to 40:60 hexanes:EtOAc, to provide intermediate **I** (2.27 g, 71%) as a white solid. ^1H NMR (500 MHz, DMSO- d_6) δ 7.83 (d, J = 8.5 Hz, 1H), 7.59 (d, J = 8.6 Hz, 1H), 6.15 (s, 1H), 4.25 – 4.16 (m, 2H), 4.05 – 3.97 (m, 2H), 3.76 (t, J = 5.8 Hz, 4H), 3.47 – 3.40 (m, 4H), 1.93 (p, J = 5.7 Hz, 2H); HRMS (QTOF) m/z calcd for $\text{C}_{14}\text{H}_{18}\text{N}_3\text{O}_3$ $[\text{M}+\text{H}]^+$ 276.1343, found 276.1343.

6-Formyl-5-(1,4-oxazepan-4-yl)picolinonitrile (J). To a solution of intermediate **I** (1.99 g, 7.23 mmol, 1 eq) in DCM (20 mL) was added TFA (20 mL), and the reaction was stirred and heated to reflux for 5 h. The mixture was concentrated in vacuo and the residue was purified by flash LC on silica gel, eluting with 60:40 to 40:60 hexanes:EtOAc, to provide intermediate **J** (1.46 g, 87%) as an off-white solid. ^1H NMR (500 MHz, DMSO- d_6) δ 9.80 (s, 1H), 7.90 (d, J = 9.0 Hz, 1H), 7.65 (d, J = 9.0 Hz, 1H), 3.82 – 3.77 (m, 2H), 3.69 – 3.64 (m, 2H), 3.64 – 3.59 (m, 2H), 3.48 – 3.43 (m, 2H), 1.89 (p, J = 5.3 Hz, 2H); LRMS (ES^+) m/z 232.2 $[\text{M}+\text{H}]^+$; HRMS (QTOF) m/z calcd for $\text{C}_{12}\text{H}_{14}\text{N}_3\text{O}_2$ $[\text{M}+\text{H}]^+$ 232.1080, found 232.1080.

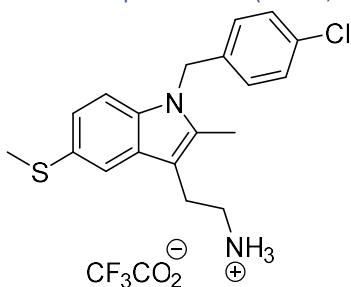
6-Acryloyl-5-(1,4-oxazepan-4-yl)picolinonitrile [TAD-0058547]. To a -78 °C solution of intermediate **J** (202 mg, 0.873 mmol, 1 eq) in THF (1.2 mL) was added a solution of 1M vinylmagnesium bromide in THF (0.9 mL, 0.9 mmol, 1 eq) dropwise. The reaction was stirred at -78 °C for 1 h, and then stirred with warming to rt for 1 h. The reaction was quenched with aqueous saturated NH_4Cl solution (10 mL) and extracted with EtOAc (3 x 25 mL). The combined organic layers were washed with brine (10 mL), dried over MgSO_4 , filtered, and concentrated in vacuo. The residue was partially purified by flash LC on silica gel, eluting with 100:0 to 97:3 DCM:MeOH, to give 136 mg of crude allylic alcohol intermediate mixed with presumed starting material. To a solution of the crude intermediate (136 mg) in DCM (5 mL) was added DMP (221 mg, 0.521 mmol), and the mixture was stirred at rt for 1 h. The mixture was concentrated in vacuo and the residue was purified by flash LC on C18-functionalized silica gel, eluting with 70:30 to 40:60 (95:5 H_2O :ACN):ACN, to provide the title product (28 mg, 12%) as a yellow gel. ^1H NMR (500 MHz, DMSO- d_6) δ 7.87 (d, J = 9.1 Hz, 1H), 7.59 (d, J = 9.1 Hz, 1H), 7.23 (dd, J = 17.4, 10.4 Hz, 1H), 6.34 (dd, J = 17.4, 1.5 Hz, 1H), 6.03 (dd, J = 10.5, 1.5 Hz, 1H), 3.80 – 3.74 (m, 2H), 3.63 (t, J = 5.2 Hz, 2H), 3.50 – 3.44 (m, 2H), 3.31 – 3.27 (m, 2H), 1.86 (p, J = 5.2 Hz, 2H); LRMS (ES^+) m/z 258.3 $[\text{M}+\text{H}]^+$; HRMS (QTOF) m/z calcd for $\text{C}_{14}\text{H}_{16}\text{N}_3\text{O}_2$ $[\text{M}+\text{H}]^+$ 258.1237, found 258.1238; LC-MS purity 97.01% (LC-MS Method A).

Synthesis of compound **14** (K116, TAD-0058616).



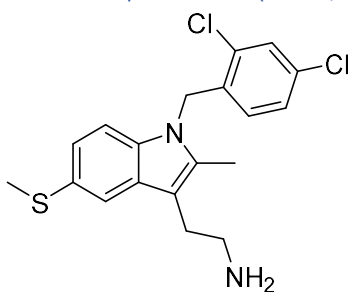
(3 α ,5 α ,6 β)-3-Aminopregnane-5,6-diol was prepared according to the procedures of Kerr et al. (WO2020028552 A1). Characterization data are consistent with those reported. ^1H NMR (400 MHz, DMSO- d_6) δ 5.84 (s, 1H), 4.60 – 4.50 (m, 1H), 3.50 – 3.40 (m, 1H), 2.18 (dd, J = 3.2, 14.4 Hz, 1H), 1.90 – 1.25 (m, 12H), 1.25 – 0.90 (m, 12H), 0.90 – 0.80 (m, 3H), 0.54 (s, 3H); LRMS (ELSD $^+$) m/z 336.2 $[\text{M}+\text{H}]^+$; LC-MS purity 99.16% (LC-MS Method C).

Synthesis of compound **15** (K149, TAD-0000088).



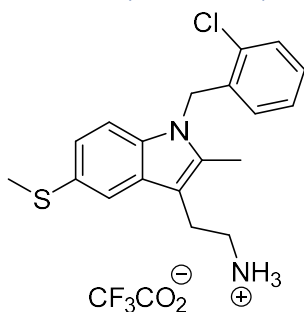
2-(1-(4-Chlorobenzyl)-2-methyl-5-(methylthio)-1H-indol-3-yl)ethan-1-aminium 2,2,2-trifluoroacetate was prepared according to the procedures of Fernandes et al⁶¹. Characterization data are consistent with those reported. ^1H NMR (400 MHz, DMSO- d_6) δ 7.72 (s, 2H), 7.52 (d, J = 1.2 Hz, 1H), 7.39 – 7.32 (m, 3H), 7.07 (dd, J = 1.6, 8.4 Hz, 1H), 7.00 (d, J = 8.4 Hz, 2H), 5.39 (s, 2H), 3.00-2.90 (m, 4H), 2.48 (s, 3H), 2.29 (s, 3H); LRMS (ES $^+$) m/z 345.16 $[\text{M}+\text{H}]^+$; LC-MS purity 99.80% (LC-MS Method B).

Synthesis of Compound **16** (K149, TAD-0000071).



2-(1-(2,4-Dichlorobenzyl)-2-methyl-5-(methylthio)-1H-indol-3-yl)ethan-1-amine [TAD-0000071]. This known compound was prepared according to the procedures of Fernandes et al⁶¹. Characterization data are consistent with those reported. ^1H NMR (400 MHz, DMSO- d_6) δ 7.69 (d, J = 2.0 Hz, 1H), 7.49 (s, 1H), 7.30 – 7.15 (m, 2H), 7.02 (dd, J = 1.2, 8.4 Hz, 1H), 6.10 (d, J = 8.4 Hz, 1H), 5.39 (s, 2H), 2.85 – 2.65 (m, 4H), 2.47 (s, 3H), 2.23 (s, 3H); LRMS (ES $^+$) m/z 379.13 $[\text{M}+\text{H}]^+$; LC-MS purity 99.25% (LC-MS Method B).

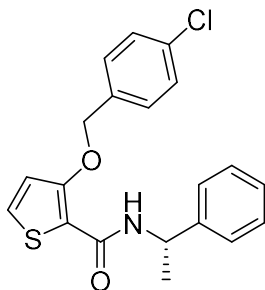
Synthesis of Compound **17** (K103, TAD-0000079).



2-(1-(2-Chlorobenzyl)-2-methyl-5-(methylthio)-1H-indol-3-yl)ethan-1-aminium 2,2,2-trifluoroacetate [TAD-0000079] was prepared according to the procedures of Fernandes et al⁶¹.

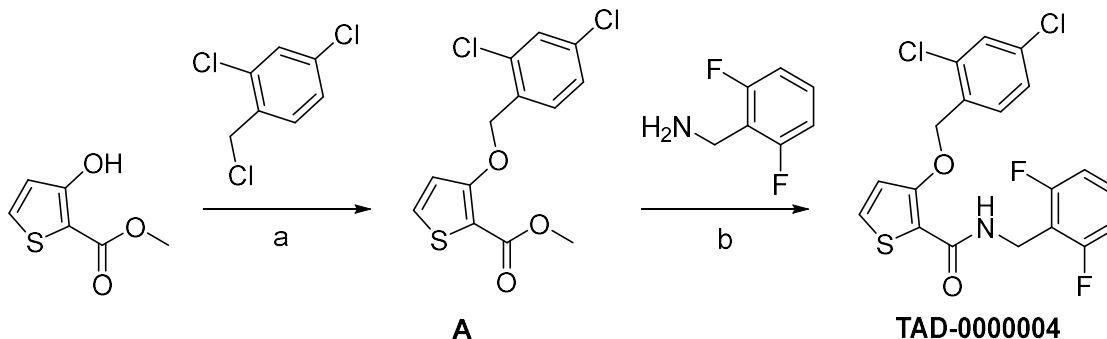
Characterization data are consistent with those reported. ¹H NMR (400 MHz, DMSO-*d*₆) δ 7.85 – 7.65 (m, 2H), 7.60 – 7.50 (m, 2H), 7.35 – 7.20 (m, 2H), 7.15 (t, *J* = 7.6 Hz, 1H), 7.10 – 7.00 (m, 1H), 6.21 (d, *J* = 7.6 Hz, 1H), 5.43 (s, 2H), 3.10 – 2.90 (m, 4H), 2.25 (s, 3H), one signal integrating to 3H obscured by solvent; LRMS (ES⁺) *m/z* 345.17 [M+H]⁺; LC-MS purity 96.88% (LC-MS Method D).

Synthesis of Compound **18** (TAD-0000014).



(S)-3-((4-chlorobenzyl)oxy)-N-(1-phenylethyl)thiophene-2-carboxamide [TAD-0000014 or AS1949490] was prepared according to the procedures of Suwa et al⁴². Characterization data are consistent with those reported. ¹H NMR (400 MHz, DMSO-*d*₆) δ 7.74 (d, *J* = 5.5 Hz, 1H), 7.60 (d, *J* = 7.9 Hz, 1H), 7.53 – 7.43 (m, 4H), 7.30 – 7.15 (m, 6H), 5.31 (s, 2H), 5.10 – 4.95 (m, 1H), 1.36 (d, *J* = 6.9 Hz, 3H); LRMS (ES⁺) *m/z* 372.03 [M+H]⁺; LC-MS purity 99.66% (LC-MS Method B).

Synthesis of Compound **19** (TAD-0000004).



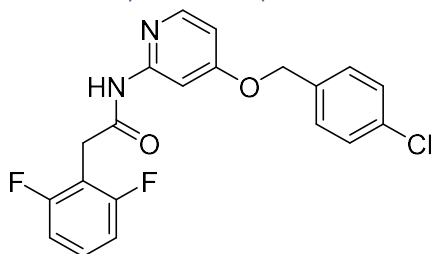
Reagents and conditions: (a) K₂CO₃, DMF, 70°C, 4h; (b) TMA, PhMe, 0°C to 80°C, 4h.

Methyl 3-((2,4-dichlorobenzyl)oxy)thiophene-2-carboxylate (A). A solution of methyl 3-hydroxythiophene-2-carboxylate (100 mg, 0.632 mmol, 1 eq) and 2,4-dichloro-1-(chloromethyl)benzene (185 mg, 0.946 mmol, 1.5 eq) and K₂CO₃ (174 mg, 1.26 mmol, 2 eq) in DMF (3 mL) was stirred at 70°C for 4h. The reaction mixture was diluted with H₂O and extracted with EtOAc. The combined organic extracts

were washed with cold H₂O and brine and dried over Na₂SO₄, filtered, and concentrated. The residue was purified by flash LC on silica gel, eluting with 93:7 to 92:8 n-heptane:EtOAc, to provide intermediate **A** (134 mg, 67%) as a white solid. ¹H NMR (400 MHz, DMSO-*d*₆) δ 7.86 (d, *J* = 5.4 Hz, 1H), 7.76 – 7.68 (m, 2H), 7.53 (d, *J* = 8.4 Hz, 1H), 7.21 (d, *J* = 5.5 Hz, 1H), 5.31 (s, 2H), 3.74 (s, 3H); LRMS (ES⁺) *m/z* 316.89 [M+H]⁺.

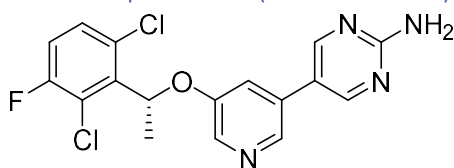
3-((2,4-Dichlorobenzyl)oxy)-N-(2,6-difluorobenzyl)thiophene-2-carboxamide [TAD-0000004 or AS1938909]. To a stirring solution of intermediate **A** (100 mg, 0.315 mmol, 1 eq) and (2,6-difluorophenyl)methanamine (58 mg, 0.405 mmol, 1.3 eq) in PhMe (3 mL) at 0°C was added a solution of 2.0M TMA in PhMe (0.236 mL, 0.472 mmol, 1.5 eq) dropwise. The reaction mixture was then stirred at 80°C for 4 h. The reaction mixture was diluted with H₂O and extracted with EtOAc. The combined organic extracts were dried over Na₂SO₄, filtered, and concentrated. The residue was purified by flash LC on silica gel, eluting with 88:12 to 85:15 n-heptane:EtOAc, to provide the title product (40 mg, 30%) as a white solid. ¹H NMR (400 MHz, DMSO-*d*₆) δ 7.76 (d, *J* = 5.5 Hz, 1H), 7.65 (d, *J* = 2.0 Hz, 1H), 7.60 (d, *J* = 8.3 Hz, 1H), 7.54 (t, *J* = 5.6 Hz, 1H), 7.48 – 7.35 (m, 2H), 7.25 (d, *J* = 5.6 Hz, 1H), 7.10 – 7.00 (m, 2H), 5.32 (s, 2H), 4.50 (d, *J* = 5.6 Hz, 2H); LRMS (ES⁺) *m/z* 427.94 [M+H]⁺; LC-MS purity 99.78% (LC-MS Method D).

Synthesis of Compound **21** (TAD-0000020).



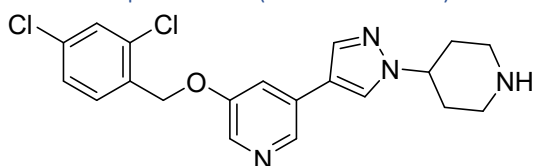
N-(4-((4-Chlorobenzyl)oxy)pyridin-2-yl)-2-(2,6-difluorophenyl)acetamide [TAD-0000020 or CPDA]. This known compound was prepared according to the procedures of Ichihara et al⁴⁵. Characterization data are consistent with those reported. ¹H NMR (400 MHz, DMSO-*d*₆) δ 10.82 (s, 1H), 8.15 (d, *J* = 5.8 Hz, 1H), 7.73 (s, 1H), 7.50 – 7.30 (m, 5H), 7.15 – 7.05 (m, 2H), 6.78 (dd, *J* = 2.3, 5.8 Hz, 1H), 5.15 (s, 2H), 3.85 (s, 2H); LRMS (ES⁺) *m/z* 389.06 [M+H]⁺; LC-MS purity 98.82% (LC-MS Method B).

Synthesis of Compound **22** (TAD-0000080).



(R)-5-(5-(1-(2,6-Dichloro-3-fluorophenyl)ethoxy)pyridin-3-yl)pyrimidin-2-amine [TAD-0000080]. This known compound was prepared according to the procedures of Lim et al⁴⁶. Characterization data are consistent with those reported. ¹H NMR (400 MHz, DMSO-*d*₆) δ 8.52 (s, 2H), 8.43 (d, *J* = 1.6 Hz, 1H), 8.10 (d, *J* = 2.4 Hz, 1H), 7.56 (dd, *J* = 5.2, 9.2 Hz, 1H), 7.50 – 7.40 (m, 2H), 6.91 (s, 2H), 6.22 (q, *J* = 6.4 Hz, 1H), 1.78 (d, *J* = 6.4 Hz, 3H); LRMS (ES⁺) *m/z* 379.10 [M+H]⁺; LC-MS purity 99.53% (LC-MS Method B).

Synthesis of Compound **23** (TAD-0000025).



3-((2,4-Dichlorobenzyl)oxy)-5-(1-(piperidin-4-yl)-1H-pyrazol-4-yl)pyridine [TAD-0000025] was prepared according to the procedures of Lim et al⁴⁶. Characterization data are consistent with those reported. ¹H NMR (400 MHz, DMSO-*d*₆) δ 8.53 – 8.47 (m, 1H), 8.42 – 8.37 (m, 1H), 8.18 (d, *J* = 2.5 Hz, 1H), 8.04 – 7.98 (m, 1H), 7.75 – 7.65 (m, 3H), 7.51 (dd, *J* = 1.7, 8.2 Hz, 1H), 5.26 (s, 2H), 4.30 – 4.10 (m, 1H), 3.15 – 2.95 (m, 2H), 2.75 – 2.55 (m, 2H), 2.10 – 1.90 (m, 2H), 1.90 – 1.70 (m, 2H); LRMS (ES⁺) *m/z* 403.10 [M+H]⁺; LC-MS purity 98.73% (LC-MS Method B).

Expression and Purification of SHIP1 and SHIP2 Proteins

Generation of hSHIP1³⁹⁵⁻⁸⁹⁸ Ptase-C2 domain and hSHIP1¹⁻⁸⁹⁹ and mSHIP1¹⁻⁸⁶¹ multidomain constructs and baculovirus P2 viral stocks: A baculovirus transfer vector (pfastBac) encoding a domain construct of human SHIP1 (hSHIP1) residues 395-898 (Uniprot Identifier: Q92835) was transposed into Bacmid DNA using DH10Bac competent cells (Fisher Scientific). P0, P1, and P2 viral stocks were generated following invitrogen's Bac-to-Bac Baculovirus expression guide. Encoded SHIP1 residues contained an N-terminal hexa-histidine tag followed by a Glutathione S-transferase (GST) solubility tag and a Tobacco Etch Virus (TEV) protease cleavage site (ENLYFQS). Baculovirus expression vectors and P2 viral stocks encoding five-domain constructs of hSHIP1 residues 1-899 and mouse SHIP1 (mSHIP1) residues 1-861 (Uniprot Identifier: Q9ES52) were generated by Genscript (Piscataway, NJ). All SHIP1 constructs generated by Genscript contained a N-terminal hexa-histidine tag followed by a linker region (GVDLGT) and a TEV protease cleavage site.

Large-scale expression of hSHIP1³⁹⁵⁻⁸⁹⁸ Ptase-C2 domain and hSHIP1¹⁻⁸⁹⁹ and mSHIP1¹⁻⁸⁶¹ multidomain constructs: Large-scale expression was performed using 500 mL of 2x10⁶ SF9 II cell/mL (viability >95%) in 2 L Erlenmeyer flasks. hSHIP1³⁹⁵⁻⁸⁹⁸ expression was initiated by transferring 1 mL of the generated hSHIP1³⁹⁵⁻⁸⁹⁸ P2 viral stock to it associated culture. Expression of hSHIP1¹⁻⁸⁹⁹ and mSHIP1¹⁻⁸⁶¹ constructs were performed similarly to hSHIP1³⁹⁵⁻⁸⁹⁸, however the volume of P2 viral stock was adjusted to achieve a Multiplicity of Infection (M.O.I) of 0.1. Viral infection took place over the course of 72 hours in a 27 °C floor shaker while shaking at 120 rpm. After the 72-hour period, the cells were centrifuged at 700 x *g* for 30 minutes, resuspended in 60 mL of Buffer A and placed at -80 °C for future use.

Large-scale purification of hSHIP1³⁹⁵⁻⁸⁹⁸ Ptase-C2 domain and hSHIP1¹⁻⁸⁹⁹ and mSHIP1¹⁻⁸⁶¹ multidomain constructs: SHIP1 constructs were purified using Immobilized Metal Affinity Chromatography (IMAC) and Gel Filtration Chromatography. Protein solutions were initially thawed at room temperature, followed by centrifugation at 75,600 x *g* for 30-45 minutes at 4 °C and passed through a 0.45 μ m nitrocellulose membrane filter. Clarified cell lysates were loaded onto a 5 mL Ni-HiTrap HP column (GE Healthcare), equilibrated in Buffer A, on an AKTA pure FPLC system set to a flow rate of 2.0 mL/min. The Ni-HiTrap HP column was initially washed with 10% buffer B to remove non-specific protein binders, and SHIP1 was eluted with 100% Buffer B. Protein concentration and purity were determined using the Bradford assay and SDS-PAGE, respectively. Fractions containing pure SHIP1 protein were mixed with 1 mg of Tobacco-etch virus (TEV) protease and placed into dialysis tubing and dialyzed against Dialysis Buffer overnight at 4 °C to facilitate removal of the N-terminal His or His-GST tag. After overnight dialysis, protein samples were passed over the 5 mL Ni-HiTrap column and unbound protein, i.e SHIP1 protein with the hexa-histidine tag removed, was collected in fractions. Any bound protein was also eluted using a 100% buffer B gradient as describe above. Fractions containing SHIP1 were pooled and concentrated for size-exclusion chromatography. Protein solutions were concentrated to 1-2.5 mL and injected onto a 24 mL Superdex 200 Increase 10/300 GL column (Cytiva) equilibrated in Buffer C. Fractions containing, pure, unaggregated SHIP1 were pooled and concentrated. Final protein concentrations were determined using Beer's law for concentration. All purified SHIP1 proteins were aliquoted out as 50 μ L aliquots at 1 mg/mL and flash frozen in liquid nitrogen.

Buffers for purification		
Buffer	Component	pH
A/Lysis/Loading [His-Trap]	50mM Tris-Base, 500mM NaCl, 5% glycerol	8.0
B/Elution [His-Trap]	50mM Tris-Base, 500mM NaCl, 5% glycerol, 400mM Imidazole	8.0
Dialysis (TEV)	50mM Tris Base, 250mM NaCl, 5% glycerol, 5mM B-ME	8.0
Sizing/storage buffer	50mM HEPES, 250mM NaCl, 5% Glycerol, 1mM TCEP	7.5

Expression and purification of hSHIP2⁴²⁰⁻⁸⁷⁸ Ptase-C2 domain from *E.coli*: The full-length human INPPL1 (Addgene, Plasmid#124645) gene was used to make the SHIP2 Ptase+C2 domain construct. For this construct, nucleotide sequence encoding amino acid residues from 420-878 were amplified using PCR and cloned into the pET21a vector. The construct had a C terminal 6x His tag. The cloning was confirmed through DNA sequencing. For recombinant protein expression and purification, the vector described above was transformed into Rosetta DE3. 12-20L of LB bacterial cultures was used. The cells were grown at 37°C (while shaking at 200rpm) until the OD was reached between 0.6-0.8. Next, the protein production was auto-induced without IPTG. The protein induction was carried out for 20 hours at 18°C (while shaking at 180rpm). Then the bacterial cells were harvested by centrifugation at 5500 rpm for 15 minutes. The bacterial pellet was dissolved with 50mM Tris, pH 8.0, 500mM NaCl, 5% glycerol, 10mM imidazole, 1mM PMSF (binding buffer). For every gram of bacterial pellet, 5mL of binding buffer was added. Next, the cells were lysed through sonication on ice. The cell lysate was then centrifuged at 14,000 rpm for 30 minutes to remove cell debris. The supernatant was incubated with Ni-NTA resin (Qiagen). The standard affinity purification protocol was followed using the Qiagen handbook. The supernatant was incubated with the Ni beads for 2 hours. And the wash buffer used was 50mM Tris, pH 8.0, 500mM NaCl, 5% glycerol, 20mM imidazole. The protein was then eluted out using 20mM Tris, pH 8.0, 150mM NaCl, 300mM imidazole. Next, the eluted protein's buffer was exchanged to 50mM Tris pH 8.0. The protein was concentrated using Millipore Amicon Ultra centrifugal filter device to a volume less than 500µL. This volume was centrifuged at 14000rpm at 4°C for 15 minutes to remove any precipitants. Next, the sample was injected into an AKTA pure 25 M FPLC. First, the protein was purified using an ion-exchange column (HiTrap Q HP). The column was equilibrated with 50mM Tris pH 8.0 prior to sample injection. The buffer A used was 50mM Tris pH 8.0, and buffer B used to generate a salt gradient was 50mM Tris 1M. The separated fractions were run on a SDS PAGE gel to determine which fractions have our protein of desire. The SDS PAGE gel was stained with Gel Code Blue to visualize the protein (**Figure 4**). The fractions containing our protein were pooled together and concentrated again

using Millipore Amicon Ultra centrifugal filter device to a volume less than 500 μ L. The purified protein was then aliquoted and flash-frozen in liquid nitrogen and stored in -80 $^{\circ}$ C.

Purity and Kinetic Characterization: The purity of proteins was assessed using SDS-PAGE and

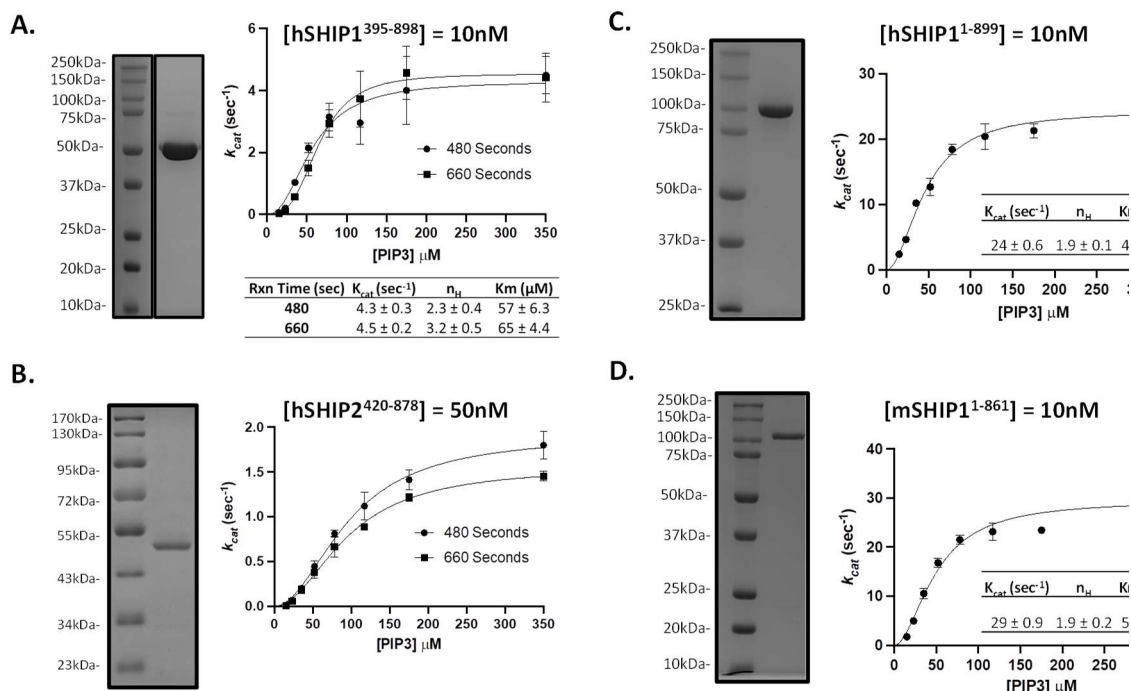


Figure 4. Purity and kinetic characterization of human and mouse SHIP1 and human SHIP2 Ptase-C2 domain proteins. Protein purity as assessed by SDS PAGE gel and stained with Gel Code or Coomassie Blue stains are shown for each protein construct to the left of the kinetic plots. The kinetic response of SHIP1 and SHIP2 constructs to PIP3 substrate are shown in each panel as labeled. All data are fit to the Hill equation.

staining gels with Gel Code Blue. Kinetic activity was assessed using PtdIns(3,4,5)P₃-diC8 as the substrate. Initial rate measurements for enzyme-mediated PtdIns(3,4,5)P₃-diC8 dephosphorylation was conducted at room temperature in a 50 mM HEPES buffer pH7.4, 150 mM NaCl, 2 mM MgCl₂. The reaction volume was 20 μ L (10 μ L substrate and 10 μ L of enzyme), and the concentration of enzyme used was 10 nM for SHIP1 and 50 nM for SHIP2. The assays were performed in 384-well plates. A maximum substrate concentration of around 10 x K_m was used and diluted through a series of 1.5 -fold dilutions resulting in 10 substrate concentrations that were used to determine k_{cat} and K_m . Enzyme concentrations used for assays were 10nM (SHIP1) or 50nM (SHIP2). To mimic the situation with compounds, enzyme was preincubated with 1 μ L DMSO (10% final concentration) at room temperature for 20 minutes. Reactions were started by adding 10 μ L PtdIns(3,4,5)P₃-diC8 solution to the enzyme + DMSO (5% DMSO final). Reaction times were 480 and 660 seconds. The reaction was stopped using 40 μ L of Biomol Green (Enzo Life Sciences). After 30 minutes of incubation at room temperature (time for the color to develop), the absorbance at 620 nm was detected using SpectraMax Me5 Microplate Spectrophotometer. A phosphate standard curve was also plotted using the phosphate standard provided by Biomol Green (Enzo Life Sciences). The slope of this standard curve was used as the conversion factor later to convert absorbance at 620nm to the concentration of phosphate (the protocol was provided by Enzo Life Sciences: Biomol green). Kinetic data were plotted as a function of substrate concentration and the steady-state kinetic parameters were obtained using SigmaPlot by fitting the data points into the Hill equation.

3.2 Evaluation of enzymatic inhibition

SHIP1 is a Mg^{2+} -dependent inositol 5'-phosphatase that converts $PI(3,4,5)P_3$ to $PI(3,4)P_2$ at the intracellular side of the cell membrane. Although our initial high-throughput screen relied on the Ptase-only catalytic domain, we used two-domain, hSHIP1³⁹⁵⁻⁸⁹⁸ and hSHIP2⁴²⁰⁻⁸⁷⁸, Ptase-C2 proteins for routine SAR studies of enzymatic inhibitory potency and selectivity because the C2 domain modulates the enzymatic activity of the Ptase¹⁷, and this protein contains both the catalytic site and a potential allosteric binding pocket at the interface between the domains. Using this protein allowed us to study both orthosteric and allosteric inhibitors. Although SHIP1 is an interfacial enzyme, we chose the soluble substrate $PtdIns(3,4,5)P_3$ -diC8. To account for the possibility that some inhibitors may have slow association rates, we preincubated compounds with the enzyme for 20 min before adding the substrate. We ran the reaction under initial velocity conditions with the substrate concentration at the K_m value to identify inhibitors (competitive, non-competitive and uncompetitive). To minimize run-to-run variability, we also optimized the reaction to produce enough phosphate so the malachite green reagent would provide sufficient signal-to-noise. Taking the initial rate and sufficient product for detection into account, we chose a 10-min reaction time. The final reaction concentration of the $PI(3,4,5)P_3$ -diC8 substrate was 52 μM , while the concentrations of the enzymes were 10 nM for SHIP1 and 50 nM for SHIP2. Reactions

were quenched with Malachite BioMol Green and then incubated for 30 min at room temperature and absorbance (620nm) measured. Inhibitory potency (IC_{50}) values were calculated by fitting absorbance versus inhibitor concentration and are reported in **Table 1** for the compounds described above. Since full-length SHIP1 contains multiple folded domains and what is predicted to be a disordered c-terminal region, expression constructs containing the ordered domains were created to assess potential differences in activity compared to the two-domain Ptase-C2 protein. Furthermore, both human and mouse (hSHIP1¹⁻⁸⁹⁹ and mSHIP1¹⁻⁸⁶¹) proteins were expressed, purified, and characterized to assess potential species differences. Enzymatic inhibitory potencies (IC_{50}) were determined for a subset of compounds as

Table 1. Enzyme inhibition of the two-domain, hSHIP1³⁹⁵⁻⁸⁹⁸ and hSHIP2⁴²⁰⁻⁸⁷⁸, Ptase-C2 proteins.

Cmpd	Name	human SHIP1 Ptase-C2					human SHIP2 Ptase-C2					Selectivity
		IC_{50} (μM)	SE	Upper (μM)	Lower (μM)	N	IC_{50} (μM)	SE	Upper (μM)	Lower (μM)	N	
1	TAD-0058585	8.99	1.07	10.3	7.9	3	166	1.09	197	141	2	18.5
2	TAD-0058656	18.6	1.05	20.4	17.0	3	>300				2	>16
3	TAD-0058581	26.8	1.08	31.5	22.8	3	>900				2	>33
5		930	1.10	1119	773	2	1700				1	1.8
6		91.9	1.10	111	76.2	2	400				1	4.3
7		44.0	1.08	51.5	37.5	3	NT				0	
9		108	1.25	168	69.6	3	>800				1	>7
13	3AC	201	1.20	291	139	13	>900				4	>4
14	K116	122	1.26	193	77.3	8	151	1.54	358	64	4	1.2
15	K160	167	1.09	196	141	3	>500				3	>3
16	K149	49.1	1.09	58.4	41.3	7	128	1.21	188	87	4	2.6
17	K103	138	1.08	162	118	3	288	1.02	302	274	2	2.1
18	AS1949490	49.6	1.25	77.3	31.8	6	>900				4	>18
19	AS1938909	37.1	1.26	59.1	23.3	6	>900				4	>24
21	CPDA	31.9	1.09	38.1	26.8	6	>900				4	>28
22	Cmpd 43	79.4	1.13	102	62.0	15	>800				5	>10
23	Cmpd 10h	251	1.13	321	197	6	252	1.06	281	225	4	1

SHIP1 and SHIP2 inhibitory potency values reported as the geometric mean of the IC_{50} (μM) with the geometric standard error, multiplicative 95% confidence limits, and number of repeats (N)

Table 2. Inhibition of human and mouse (hSHIP11-899 and mSHIP11-861) enzymes.

Cmpd	Name	human SHIP1 SH-PH-Ptase-C2					mouse SHIP2 SH-PH-Ptase-C2					N
		IC_{50} (μM)	SE	Upper (μM)	Lower (μM)	N	IC_{50} (μM)	SE	Upper (μM)	Lower (μM)	N	
1	TAD-0058585	21.5				1						
2	TAD-0058656*	125.0	7.62	7253.3	2.2	2	> 952					
3	TAD-0058581*	148.3	6.42	6111.5	3.6	2	> 952					1
13	3AC	740.8	1.15	981.8	558.9	9	473.4	1.72	1403.0	159.7	2	
14	K116	87.0	1.24	133.4	56.8	4	119.1	1.34	212.3	66.8	2	
15	K160*	150.7	1.11	185.1	122.7	2	155.0					1
16	K149	47.9	1.03	50.5	45.5	2	50.6					1
17	K103	144.9	1.86	503.1	41.7	4	80.5					1
18	AS1949490*	409.3	2.33	2214.1	75.7	2	> 952					1
19	AS1938909*	360.3	1.70	1038.6	125.0	3	> 952					1
21	CPDA*	153.4	2.08	663.2	35.5	2	> 952					1
22	Cmpd 43	75.1	1.15	99.9	56.4	10	83.8	1.26	134.0	52.4	2	
23	Cmpd 10h	193.1	1.31	329.5	113.2	5	300.4	1.03	317.9	283.9	2	

Human and mouse SHIP1 SH-PH-Ptase-C2 inhibitory potency values reported as the geometric mean of the IC_{50} (μM) with the geometric standard error, multiplicative 95% confidence limits, and number of repeats (N). *Compounds with poor solubility in the assay.

described above with the following changes: the reaction time was 2 min and the substrate concentration was 40 μ M. The results are reported in **Table 2**.

Enzyme assay validation and quality control

Plate uniformity: Assay conditions were experimentally optimized for 384 well plates.

Signal window and Z' control charting: The upper and lower boundaries (*i.e.* signal window) and Z' of the enzyme measurements are collected from each assay plate.⁵⁷ See **Tables 9-12**.

Minimum Significant Ratio (MSR): The MSR is defined as the smallest ratio between the potencies of two compounds that is statistically significant and is calculated as $MSR = 10^{2\sqrt{2}s}$, where s is an estimate of the standard deviation of a log potency for one compound.⁵⁸ A replicate-experiment MSR was estimated from independent runs of 20-30 compounds and is calculated as $MSR = 10^{2sd}$, where sd is the standard deviation of the paired differences in log potency across the two runs. See results in **Tables 9-12**.

Table 3. SHIP1 Ptase-C2 enzyme assay validation statistics

SHIP1 Ptase-C2	Signal window	Z' factor	MSR Study 1 vs Study 2	MSR Study 1 vs Study 3	MSR Study 2 vs Study 3
Study 1	2.964	0.721			
Study 2	4.064	0.564	1.87	1.88	1.67
Study 3	4.301	0.705			

Table 4. SHIP2 Ptase-C2 enzyme assay validation statistics

SHIP2 Ptase-C2	Signal window	Z' factor	MSR Study 1 vs Study 2	MSR Study 1 vs Study 3	MSR Study 2 vs Study 3
Study 1	3.955	0.714			
Study 2	3.067	0.653	3.92	3.23	2.81
Study 3	4.115	0.756			

Table 5. Human SHIP1 five-domain enzyme assay validation statistics

Human SHIP1	Signal window	Z' factor	MSR Study 1 vs Study 2
Study 1	2.809	0.469	
Study 2	2.966	0.822	1.78

Table 6. Mouse SHIP1 five-domain enzyme assay validation statistics

Mouse SHIP1	Signal window	Z' factor	MSR Study 1 vs Study 2
Study 1	2.696	0.682	
Study 2	3.407	0.772	2.12

3.3 Demonstration of target engagement in cells

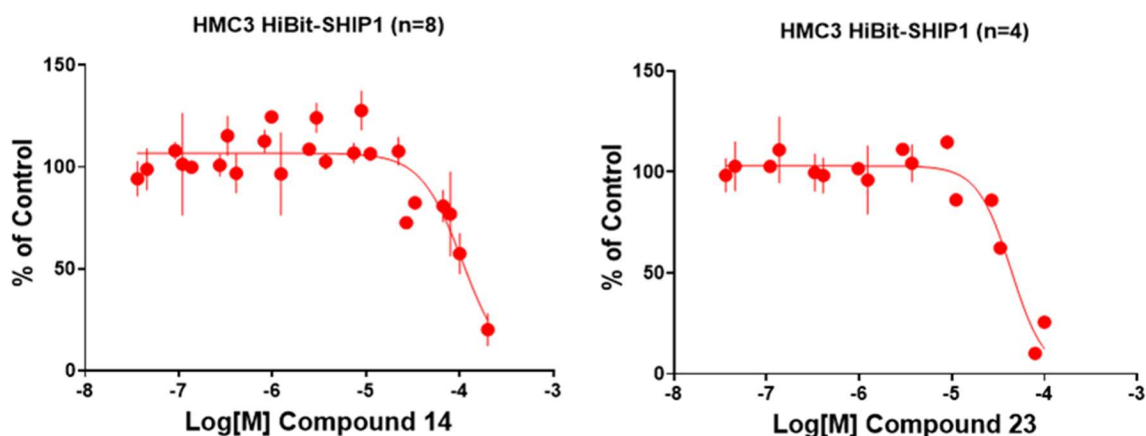


Figure 5 Cellular Thermal Shift Assay (CETSA) results for SHIP1 inhibitors **14** and **23**, demonstrating significant thermal destabilization. Luminescence data normalized to DMSO-treated control samples at 37 °C, which were arbitrarily set to 100.

The multidomain and multifunctional nature of SHIP1 carries certain risks to lead optimization efforts, specifically differences between cell-free enzyme assays and cellular potencies can confound interpretation of SAR^{26,27}. Therefore, we enabled a cellular target engagement assay to provide evidence that observed pharmacological activities were on target^{47,48}. Cellular Thermal Shift Assays (CETSA) have become routine to assess cell-based target engagement by quantifying changes in protein thermal stability upon ligand binding to endogenous proteins in intact cells⁴⁹. A split Nano Luciferase (SplitLuc CETSA) version of the assay was used to provide sufficient throughput for SAR studies^{50,51}. HMC3 cells were stably transfected with HiBit-INPP5D to express full-length human SHIP1 protein in a physiologically relevant cellular context. The thermal stability of this HiBit-labeled protein in intact cells was measured in two formats. In screening mode cells were treated with a single concentration of compound (40-100 μ M) or fragments (200 μ M) at 37 °C for 60 min and then exposed to 3-min isothermal heating at 44.2 °C, the experimentally determined T_m of HiBit-SHIP1 (n=28). In dose-response mode, cells were treated with decreasing concentrations from 100 μ M (compounds) or 200 μ M (fragments) with 1:3 serial dilutions to generate a percent of control 8-point curve. An AC_{50} was calculated using a four-parameter logistic curve

Table 7. Cellular Thermal Shift Assay (CETSA) and AKT signaling assay.

Cmpd	Name	CETSA			Signaling				N
		AC_{50} (μ M) ¹	% ²	TE ³	IC_{50} (μ M) ⁴	SE	Upper	Lower	
1	TAD-0058585	NC	92	No	> 60				1
2	TAD-0058656	46 \pm 5 (2)	30 \pm 7 (2)	Yes	12.4	1.36	22.98	6.72	2
3	TAD-0058581	173	63 \pm 12 (2)	Yes	5.60	1.34	10.01	3.13	2
5		NT	NT	-					
6		NT	NT	-	> 60				1
7		NC	77	No	> 60				1
9		41	5	Yes	> 60				1
13	3AC	NT	NT	-					
14	K116	97 \pm 16 (4)	40 \pm 20 (4)	Yes	2.93	1.12	3.7	2.3	1
15	K160	46	14	Yes	5.82	1.06	6.54	5.18	2
16	K149	NT	NT	-	4.11	1.12	5.17	3.27	2
17	K103	89 \pm 11 (2)	46 \pm 21 (2)	Yes	4.59	1.14	6.00	3.52	2
18	AS1949490	NC	84	No	37.9				1
19	AS1938909	NC	75 \pm 0 (2)	No	>60				1
21	CPDA	NC	92 \pm 5 (2)	No	28.0				1
22	Cmpd 43	NC	92	No	5.85	1.14	7.58	4.52	2
23	Cmpd 10h	54 \pm 15 (3)	27 \pm 15 (3)	Yes	6.52	1.03	7.06	6.16	2

1. Concentration (μ M) that induced a half-maximum loss of luminescence (AC_{50}) compared to control. 2. Percent luminescence at highest dose (100 μ M). 3. Target engagement (TE) was considered significant if ΔT_m difference from control at highest dose was >3SD, otherwise AC_{50} was not calculated (NC). NT = not tested. Reduction in the ratio pAKT/tAKT determined by Alpha SureFire assay and reported as the geometric mean of the IC_{50} (μ M) with the geometric standard error, multiplicative 95% confidence limits, and number of repeats (N).

The thermal stability of this HiBit-labeled protein in intact cells was measured in two formats. In screening mode cells were treated with a single concentration of compound (40-100 μ M) or fragments (200 μ M) at 37 °C for 60 min and then exposed to 3-min isothermal heating at 44.2 °C, the experimentally determined T_m of HiBit-SHIP1 (n=28). In dose-response mode, cells were treated with decreasing concentrations from 100 μ M (compounds) or 200 μ M (fragments) with 1:3 serial dilutions to generate a percent of control 8-point curve. An AC_{50} was calculated using a four-parameter logistic curve

regression model. Percent luminescence remaining at the highest concentration is also reported for the compounds when the difference from the DMSO control is greater than 3x the standard deviation (SD). Otherwise, an AC₅₀ was not calculated. Results are reported in **Table 7** and example concentration response curves for compounds **14** and **23** are shown in **Figure 5**.

Cellular Thermal Shift Assay (CETSA) validation and quality control

Melting temperature (T_m) of HiBit-SHIP1 determined experimentally: Multiple experiments using a 12-point (in each row of the 96 well PCR plate) temperature gradient (38—52 °C) heating (3 min) were performed to determine the melting temperature (T_m) of HiBit-SHIP1. Results in **Figure 6** demonstrate that 44.2 °C is the T_m for HiBit-INPP5D in the HMC3 stable clone. Therefore, 44.2 °C was used in isothermal CETSA screening for both the single point and compound concentration response studies. Raw luminescence data are normalized to signal mean of MAX (initial 3 wells, 38 °C, 38.3 °C and 39.2 °C) in the same plate. Normalized data are calculated as %Max=100*X/mean of Max wells.

CETSA with HiBit Control Protein: A control CETSA with 1 nM of the HiBit Control Protein (Promega, Cat N301A) was established to detect non-specific binding or interference in the assay system. All assay conditions following the same protocol except for replacing cells expressing HiBit-INPP5D with the HiBit control protein. Example results from compound **23** are shown in **Figure 7**, which verify the dose dependent response in **Figure 3** is SHIP1 dependent and not due to non-specific binding or interference.

Plate uniformity: Assay conditions were experimentally optimized for 96 well PCR plates, including cell plating density and volume (HMC3/HiBit-INPP5D stable clone), compound treatment time, and luminescence signal detection (NanoGlo lytic detection kit from Promega). All liquid transfer procedures using an automatic liquid pipetting system (OPENTRONS, OT2), and data analysis, were performed as described above. A plate uniformity test was performed on plates of High signal (37 °C heating), Mid signal (44.2 °C heating, the T_m of HiBit-SHIP1) and Low signal (50 °C heating) respectively. Results are shown in **Figure 8**. Raw luminescence signal of the 3 plates shews CV<20%, met uniformity requirement. Z' of High vs. Low and Mid vs. Low are all>0.4 met requirements for quantitative assay. Z' of High vs. Mid >0.4 when the assay runs in triplicates that will be the condition for single point compound screening.

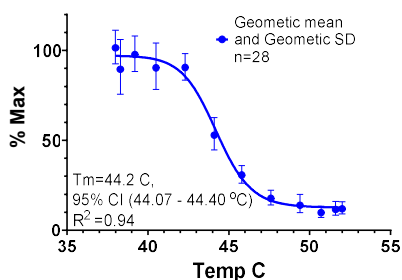
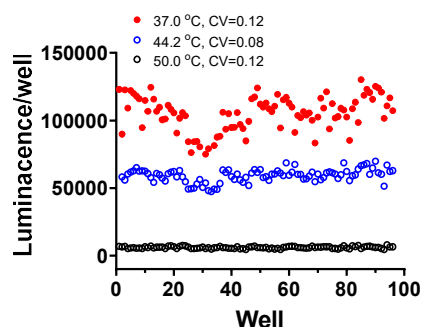


Figure 6. HMC3 HiBit-INPP5D CETSA T_m.



	37C	44.2C	50C
Ave.	106833.44	59249.3	6028.2
SD	11398.333	4875.2	748.3
CV	0.107	0.082	0.124
Z', n=1	-0.03	0.68	0.64
Z', n=2	0.274	0.769	0.744
Z', n=3	0.408	0.817	0.791
	37C:44.2C	44.2C:50C	37C:50C

Figure 8 HMC3 HiBit-INPP5D CETSA plate uniformity.

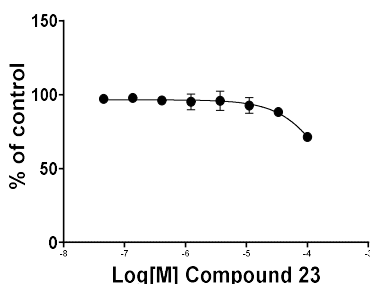


Figure 7. CETSA with HiBit Control Protein (n=2).

3.4 Cellular pharmacology

SHIP1 modulates AKT signaling because it converts PI(3,4,5)P₃ to PI(3,4)P₂ and both phosphatidylinositols bind and activate PH-containing proteins such as PDK1 and AKT^{11,18,52-54}. Therefore we established an AKT signaling assay in THP1 cells to provide further evidence of on-target activity. Cells were treated with inhibitors for 90 minutes and then the levels of phosphorylated and total AKT (pAKT/tAKT) were detected using the Perkin Elmer Alpha SureFire Ultra Multiplex PhosphoAKT (S473) kit. Results are reported in **Table 7** and example concentration response curves for compounds **14** and **23** are shown in **Figure 9**. Reduction in AKT phosphorylation was consistently observed in this cellular context when target engagement was confirmed by CETSA except for compound **22**, a notable outlier that potentially reduced pAKT but failed to destabilize the HiBit-SHIP1 protein.

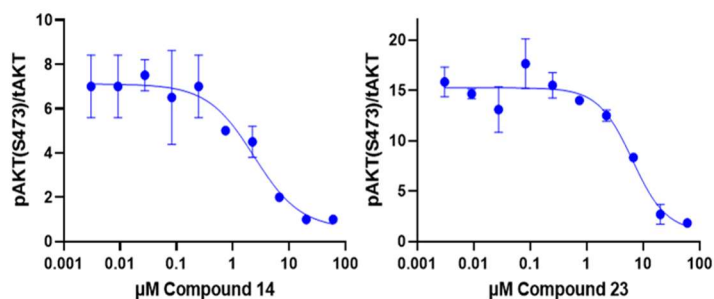


Figure 9 Ratio of S473 phosphorylated AKT to total AKT concentration response curves. Concentration response curves of the ratio pAKT(S473)/tAKT determined by Alpha SureFire assay.

Compounds that demonstrated significant cellular target engagement and changes in AKT signaling were evaluated in a phenotypic high-content imaging assay with simultaneous measures of phagocytosis, cell number, and nuclear intensity to assess both cellular pharmacology and cell health in

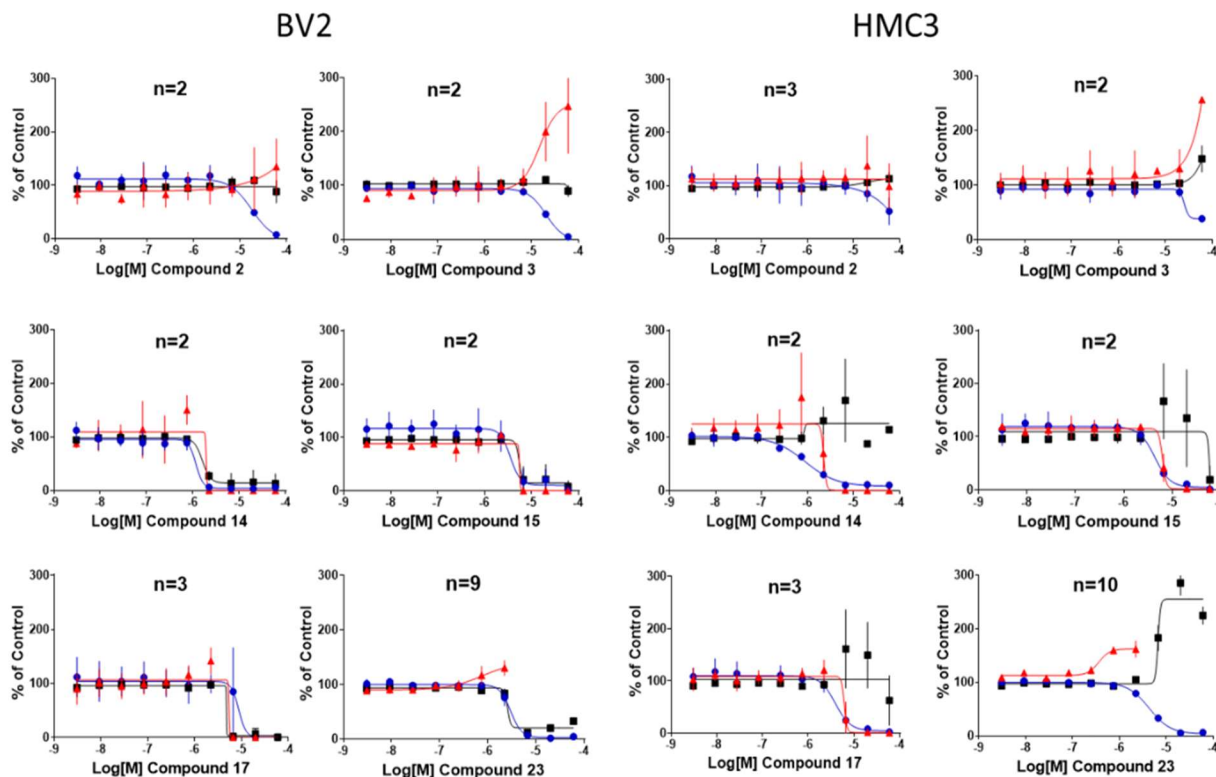


Figure 10 Effect of SHIP1 inhibitors on Cell Count (■), Nuclear Intensity (■), and Phagocytosis (▲) in BV2 and HMC3 cells.

Cmpd	Name	Cell Count				Nuclear Intensity				Phagocytosis				N
		IC ₅₀ (μ M)	SE	Upper (μ M)	Lower (μ M)	IC ₅₀ (μ M)	SE	Upper (μ M)	Lower (μ M)	EC ₅₀ (μ M)	SE	Upper (μ M)	Lower (μ M)	
2	TAD-0058656	17.5	1.02	18.3	16.9	20.1	2.99	179	2.24	33.0	1.82	109	10.0	2
3	TAD-0058581	21.0	1.06	23.7	18.5	>60	NC	NC	NC	20.8	2.87	171	2.53	2
14	K116	1.22	NC	NC	NC	1.92	NC	NC	NC	NC	NC	NC	NC	1
15	K160	3.55	1.34	6.36	1.98	5.09	1.24	7.83	3.30	NC	NC	NC	NC	2
17	K103	7.0	1.69	20.1	2.46	4.98	1.12	6.27	3.95	0.90	3.58	11.57	0.07	3
23	Cmpd 10h	4.19	1.35	7.63	2.30	5.18	1.50	11.70	2.30	1.94	1.14	2.54	1.49	3

Table 8. Potencies of SHIP1 inhibitor treatment of HMC3 Cells on Cell Count (IC₅₀), Nuclear Intensity (IC₅₀), and Phagocytosis (EC₅₀). Values reported as the geometric mean of the IC₅₀ or EC₅₀ (μ M) with the geometric standard error, multiplicative 95% confidence limits, and number of repeats (N).

Cmpd	Name	Cell Count				Nuclear Intensity				Phagocytosis				N
		IC ₅₀ (μ M)	SE	Upper (μ M)	Lower (μ M)	IC ₅₀ (μ M)	SE	Upper (μ M)	Lower (μ M)	EC ₅₀ (μ M)	SE	Upper (μ M)	Lower (μ M)	
2	TAD-0058656	41.9	1.43	85.9	20.5	35.5	1.69	101	12.4	NC	NC	NC	NC	2
3	TAD-0058581	49.1	1.22	73.3	32.9	58.5	1.03	61.5	55.7	>60	NC	NC	NC	2
14	K116	1.02	NC	NC	NC	1.04	NC	NC	NC	0.117	NC	NC	NC	1
15	K160	4.54	1.36	8.44	2.44	9.64	2.10	42.3	2.20	NC	NC	NC	NC	2
17	K103	4.02	1.14	5.19	3.12	5.41	2.35	30.0	0.98	2.54	2.63	17.6	0.366	3
23	Cmpd 10h	5.18	1.12	6.55	4.10	9.84	1.43	20.1	4.82	0.767	2.82	6.08	0.0967	3

Table 9. Potencies of SHIP1 inhibitor treatment of BV2 Cells on Cell Count (IC₅₀), Nuclear Intensity (IC₅₀), and Phagocytosis (EC₅₀). Values reported as the geometric mean of the IC₅₀ or EC₅₀ (μ M) with the geometric standard error, multiplicative 95% confidence limits, and number of repeats (N).

parallel³². Model cell lines BV2 and HMC3 were used to provide adequate throughput. Microglia isolated from mouse brain were used to verify that results from the BV2 and HMC3 cells are mechanistically similar to those obtained with primary cells. Cells were treated with compounds for 24 hrs and then seeded with pHrodo-dye labeled myelin. After 20 hrs, nuclear staining solution was added, and the plates were incubated for another 30 min and then scanned with an ArrayScan XTI high-content analysis reader (Thermo Scientific), and the associated image data was analyzed with Thermo Scientific HCS Studio. Nuclei were stained with Hoechst 33342 just before final high content imaging scan. Since the assay is mix-and-read without liquid change, the imaging cell count is reliable. Mean total phagocytosis spot intensity per cell, total cell counts per well, and mean average nuclear intensity per cell for cell health were measured. Cellular potencies for each endpoint (EC₅₀ for phagocytosis, IC₅₀ for cell count) were calculated using a four-parameter logistic curve regression model. Results are described in **Figure 10** and **Tables 8** and **9** and for compounds that demonstrated cellular target engagement as determined by CETSA.

Increased uptake of pHrodo-myelin, calculated as an EC₅₀, is interpreted as a measure of microglial phagocytosis activation. Decreased cell count, calculated as an IC₅₀, is interpreted as decreased cellular proliferation and cell loss caused by mechanisms such as apoptosis. Cell counts are increased (calculated as an EC₅₀) or nuclear intensity decreased (calculated as an IC₅₀). The nature of these changes in cell count

or nuclear intensity may be interpreted as early or late apoptosis, but further study such as TUNEL and caspase activation would be required to confirm. Compound **2** was inactive, demonstrating changes in BV2 and HMC3 cellular phenotypes only at the highest concentrations, consistent with high-dose cytotoxicity. Compound **3** increased phagocytosis at high concentrations probably due to cell stress; however, BV2 cell counts were reduced, and early apoptosis may have been induced in HMC3 cells. Compound **14** may have caused late apoptosis of BV2 cells, as suggested by a reduction in cell count and nuclear intensity with an IC_{50} of 1 μ M. In HMC3 cells, compound **14** decreased cell counts without increasing phagocytosis. The phenotype arising from treatment with compounds **15** and **17** was similar to that observed with compound **14**, although the effects of **17** were milder and are worth further investigation. Compound **23** consistently induced phagocytosis of both BV2 and HMC3 cells at concentrations that did not result in significant changes in either cell count or nuclear intensity. At high concentrations cell counts were reduced and the compound appeared to induce late apoptosis (decreased nuclear intensity) in BV2 cells but early apoptosis (increased nuclear intensity) was induced in HMC3 cells. Since compound **23** increased phagocytosis in the BV2 mouse microglial cell line 1.2–2-fold over baseline at concentrations of 1–2 μ M with minimal effects on cell health, we tested its ability to activate primary mouse microglia isolated from neonate mice. Compound **23** increased phagocytosis 1.5-fold at concentrations that did not result in significant changes in either cell count or nuclear intensity up to 2.2 μ M with a half maximal effective concentration (EC_{50}) of 540 nM (Figure 11).

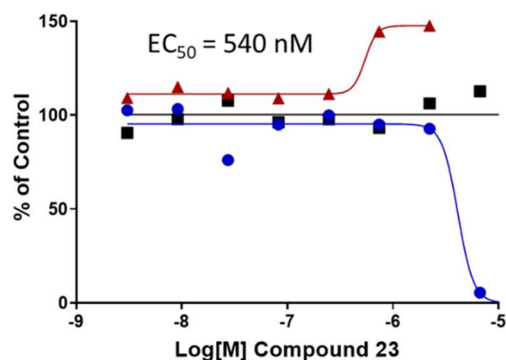


Figure 11 Activity of a SHIP1 inhibitor in primary mouse microglia. Compound 23 induced phagocytosis at concentrations that did not result in significant changes in either cell count or nuclear intensity.

Microglial Phagocytosis assay validation and quality control

Plate uniformity: Assay conditions were experimentally optimized for 384 well plates, including cell plating density, compound treatment time, pHrodo-myelin seeding concentration and time, and cell staining. All liquid transfer and compound serial dilutions with automation (multidrop and an automatic liquid handler), as well as high content imaging settings and data analysis, were performed as described above. Plate uniformity test with a 384 well plate was performed focusing on phagocytosis measurements on HMC3 and BV2, each cell line plated into half of the plate (192 wells) for Max signal (96 wells with pHrodo seeding) and 96 wells for Min signal (without the seeding). Results are shown in **Figure 12**: 1) CV <20% from all wells of Max phagocytosis signal (mean spot total intensity per cell) of both HMC3 and BV2 that meet plate uniformity requirement; 2) $Z' > 0.4$ (Max vs Min) from both HMC3 and BV2 when the assay run with duplicates (n=2) that meet the requirement as well.

Z' control charting: The Z' of the phagocytosis measurements are collected from each assay plate based on data of Max (32 wells in columns 12 and 23) and Min (32 wells in columns 1 and 24). Recorded Z' control charting is shown in **Figure 13**; results indicated that every assay plate with $Z' > 0.4$ that met quality requirement during operation.

Assay plate design: For testing compound potency, a 384 well assay plate is set with column 1 and 24 as Min controls (no pHrodo-myelin seeding), the rest of the wells are all with the seeding including wells of column 12 and 23 as untreated controls and wells in columns 2-11, 13-22 for 10-point serial diluted compound treatments in duplicates so that each plate can test 16 compounds for AC_{50} .

Potency charting of a control compound: The PI3K δ inhibitor idelalisib was selected as reference based on its highly reproducible inhibition of phagocytosis in the assay. The phagocytosis measurement was normalized to untreated wells as “%control=100*X/mean of control wells” (where X is raw phagocytosis

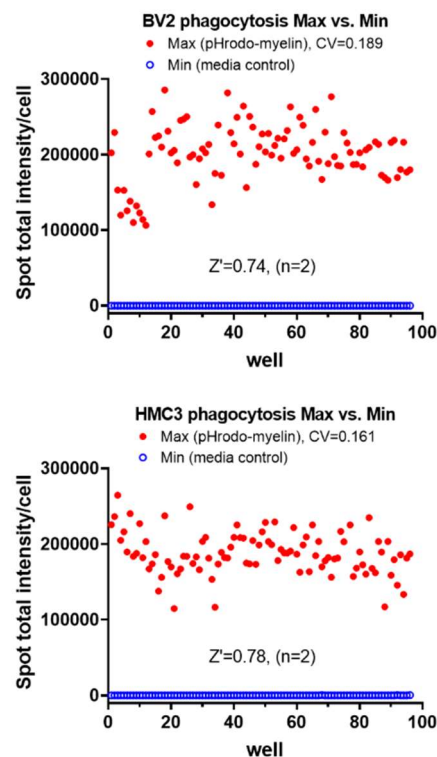


Figure 12. Microglial Phagocytosis Assay Plate Uniformity.

signal from a testing well), so that wells with no effect show quantitation around 100%, a compound of stimulating show >100% and inhibition <100%. The IC₅₀ of Idelalisib control charting is shown in **Figure 14**, which serves as a quality control of the phagocytosis assay.

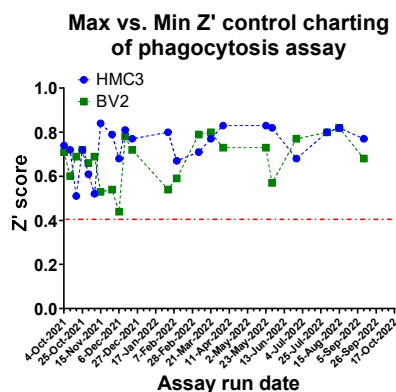


Figure 13. Microglial Phagocytosis Assay Z' Control Charting.

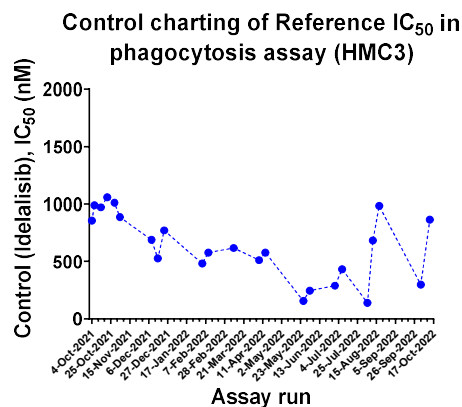


Figure 14. Microglial Phagocytosis Assay Potency Charting of Control Idelalisib.

In addition to the phagocytosis measurement as main output, the high content assay also collects total cell number (cell number/well) and average nuclear DNA intensity (Nuclear Intensity) for profiling to help evaluate compound cytotoxicity.

3.5 Pharmacokinetics

To assess the suitability of compound **23** for animal studies, *in silico* ADME properties were determined using ADMET Predictor 10.2 (**Table 10**). The reliability of AP to calculate these properties has been recently reviewed⁵⁵. We then determined physicochemical and ADME properties in the following assays: kinetic solubility, microsomal stability intrinsic clearance (CL_{int}) in mouse liver microsomal solution, MDCK permeability (P_{app}), and protein binding (f_u) in mouse plasma and brain (**Table 11**). Plasma PK profiles were predicted using GastroPlus 9.8.2 from chemical structure and *in vitro*-derived plasma fraction unbound (f_u), NADPH-mediated clearance in mouse liver microsomes (CL_{int}), and MDCK permeability (P_{app}). Projected PK profiles for 10 and 100 mg/kg oral doses in mouse are shown in **Figure 7** (dotted lines). We then conducted a

single-dose pharmacokinetic (PK). The compound was formulated at 5 mg/ml in HPMC (1%)/Tween 80 (0.25%)/purified water. Male C57BL/6J mice aged 8–12 weeks from The Jackson Laboratory (Jax #000664;

Lipophilicity ¹	cLogD	2.04
Solubility ²	Sw (mg/mL)	0.441
Permeability ³	MDCK (x10 ⁻⁶ cm/s)	73.2
Metabolism ⁴	RLM Clint (μL/min/mg)	132
Blood Brain Barrier	LogBB ⁵	0.637
	BBB Filter ⁶	Low
	Pgp Substrate ⁷	No
	Pgp Inhibition ⁸	Yes

Table 10 *in silico* ADME properties of Compound **23**

Calculated using ADMET Predictor v10.2. 1. Octanol-water distribution coefficient (from pKa and cLogP); 2. Native water solubility; 3. Apparent MDCK permeability (P_{app}); 4. Estimated intrinsic clearance rat liver microsomes for predicted sites of metabolism; 5. Log brain/blood partition coefficient; Blood brain barrier parameters predicting the likelihood of 6. Crossing the BBB, 7. P-gp efflux, and 8. P-gp inhibition.

n=3-4) were dosed (10 mg/kg, and 100 mg/kg) via oral gavage (20 ml/kg). Plasma exposures were obtained at 0.5, 1, 2, 4, 8, and 12 hr and 24 hr. At the 10 mg/kg dose, brain exposures were determined at 8 hrs. At the 100 mg/kg dose, brain exposures were obtained at terminal 2, 4, and 24 hrs. Measured and average exposures (solid lines) are depicted in **Figure 7** and corresponding PK parameters are reported.

All *in vivo* animal studies were approved by the Institutional Animal Care and Use committee (IACUC) at The University of Pittsburgh (PITT) prior to initiation.

Adult male C57BL/6J mice (JAX stock# 000664) were received from The Jackson Laboratory at approximately 8 weeks of aged and acclimated for at least 1 week to the University of Pittsburgh animal facility prior to the experiments. Mice were group housed (n=3-4 per cage) with *ad libitum* access to food and water. The housing room consists of ventilated caging and automated watering system with room temperature controlled at a setting of 72±2°F and humidity at 50±10%.

The testing facility was on a 12:12 L:D schedule (lights on at 7:00 am). Pharmacokinetic studies were conducted in non-fasted subjects with compounds administered at the beginning of the light cycle. Mice were dosed (10 mg/kg, and 100 mg/kg) via oral gavage (20 ml/kg formulated at a 5 mg/mL dose volume in a vehicle solution of 1% hydroxypropylmethylcellulose (HPMC)/Tween 80 (0.25%)/purified water^{59,60}. Serial blood samples (50 µL) were collected via the tail sampling procedure into heparinized capillary tubes at 0.5, 1, 2, 4, 8, and 12 hr and 24 hr post dosing. Blood was transferred into Eppendorf tubes maintained on wet ice and plasma was processed within 20-60 min post blood collection by centrifugation at 14500 rpm for 10 minutes at 4°C. Plasma aliquots were frozen on dry ice and stored at -80C until analysis. For terminal tissue collection, mice were subjected to isoflurane anesthesia to the surgical plan of anesthesia followed by decapitation and brain removal. Brains were briefly rinsed in cold PBS and snap frozen on dry ice followed by storage at -80C until processing and analysis. At the 10 mg/kg dose, brain exposures were determined at 8 hrs. At the 100 mg/kg dose, brain exposures were obtained at terminal 2, 4, and 24 hrs.

Solubility ¹	Last soluble (µM)	41
	First insoluble (µM)	60
Metabolism ²	MLM Clint (µL/min/mg)	28.9
Permeability ³	MDCK (x10 ⁻⁶ cm/s)	10.9
Protein Binding ⁴	Plasma (fu)	0.0184
	Brain (fu)	0.0014

Table 11. Physicochemical and *in vitro* ADME properties of Compound 23

1. Kinetic solubility in pH 7.4 phosphate buffer. 2. Intrinsic clearance in mouse liver microsomes. 3. MDCK Permeability assay as an estimate of intestinal absorption (Papp); 4. Mouse plasma and brain fraction unbound (fu).

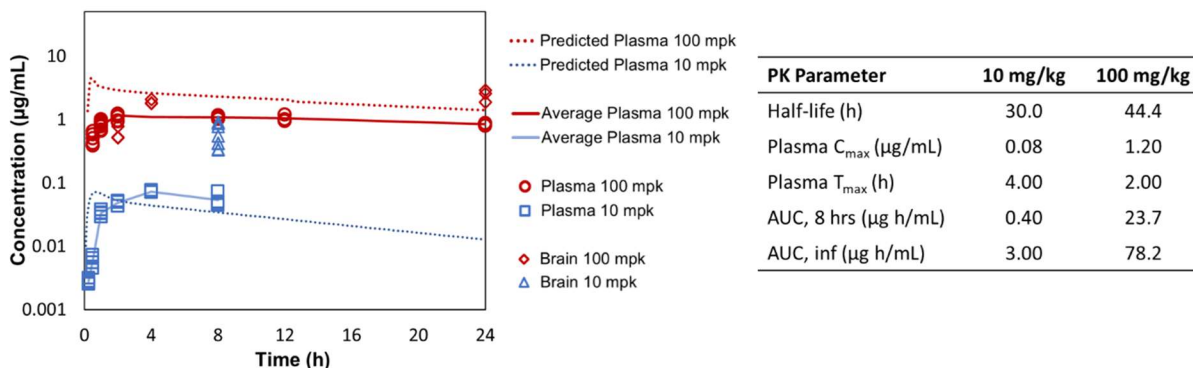


Figure 15. Pharmacokinetics. Compound **23** demonstrated significant exposures in both plasma and brain with a brain/plasma ratio of 0.5–3-fold that increased over time.

4 DISCUSSION

The goal of this work was to assess SHIP1 inhibitors with new assays and a novel strategy to ensure target engagement in cells and for animal studies. **Figure 16** outlines the assays developed and **Table 12** summarizes results for each compound in each assay. The differences observed between the SHIP1 Ptase-C2 and the human and mouse multi-domain forms of the protein demonstrate that the protein construct selected for enzyme assays is crucial and the lack of correlation to cellular potencies indicates further studies are required to identify the best protein construct for biochemical assays. Given the complexity of the protein and difficulties translating a cell-free enzyme assay to cellular pharmacology, we executed a strategy using a combination of (CETSA) and target dependent signaling (pAKT) to provide evidence that cellular effects are mediated through SHIP1. The CETSA cellular target engagement assay provided crucial evidence that observed pharmacological activities were on target. Only about half of the compounds that inhibited the cell-free enzyme demonstrated significant cellular target engagement, consistently

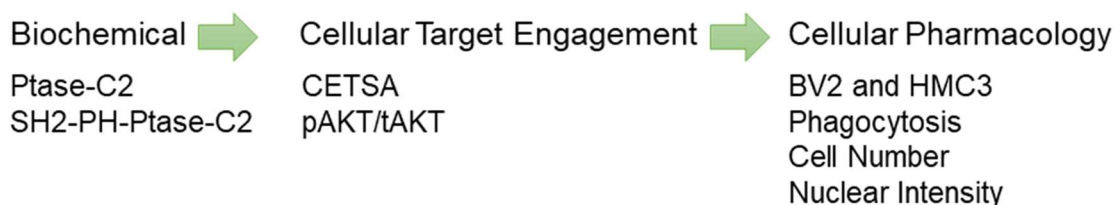


Figure 16 Testing flow of assays

Cmpd	Name	TAD	Enzyme ¹		CETSA ²		AKT ³	BV2			HMC3			Assessment
			SHIP1 IC ₅₀ (μM)	SHIP2 IC ₅₀ (μM)	AC ₅₀ (μM)	%		Cell IC ₅₀ (μM)	Nuc IC ₅₀ (μM)	Phago EC ₅₀ (μM)	Cell IC ₅₀ (μM)	Nuc IC ₅₀ (μM)	Phago EC ₅₀ (μM)	
1	HTS C4	TAD-0058585	8.99	166	NC	92	> 60.0	-	-	-	-	-	-	No target engagement by CETSA
2	HTS C10	TAD-0058656	18.6	>300	46	30	12.43	17.5	20.1	33.0	41.9	35.5	NC	Target engaged; does not induce phagocytosis
3	HTS C12	TAD-0058581	26.8	>900	173	63	5.60	21.0	>60	20.8	49.1	58.5	>60	Target engaged; does not induce phagocytosis
13	3AC	TAD-0000635	201	>900	NT	NT	-	-	-	-	-	-	-	Not fully assessed
14	K116	TAD-0058616	122	151	97	40	2.93	1.26	1.26	NC	0.97	1.07	NC	Target engaged; cytotoxic
15	K160	TAD-0000088	167	>500	46	14	5.82	3.55	5.09	NC	4.54	9.64	NC	Target engaged; cytotoxic
16	K149	TAD-0000071	49.1	128	NT	NT	4.11	-	-	-	-	-	-	Not fully assessed
17	K103	TAD-0000079	138	288	89	46	4.59	7.0	4.98	0.90	4.02	5.41	2.54	Target engaged; mild phagocytosis and cytotoxicity
18	AS1949490	TAD-0000014	49.6	>900	NC	84	37.9	-	-	-	-	-	-	No target engagement by CETSA
19	AS1938909	TAD-0000004	37.1	>900	NC	75	> 60.0	-	-	-	-	-	-	No target engagement by CETSA
21	CPDA	TAD-0000020	31.9	>900	NC	92	28	-	-	-	-	-	-	No target engagement by CETSA
22	Cmpd 43	TAD-0000080	79.4	>800	NC	92	5.85	-	-	-	-	-	-	No target engagement by CETSA
23	Cmpd 10h	TAD-0000025	251	252	54	27	6.59	4.19	5.18	1.94	5.18	9.84	0.767	Target engaged; phagocytosis without cytotoxicity

Table 12 1) Human SHIP1 and SHIP2 two domain protein (2D = Ptase-C2) inhibitory potency reported as geometric mean of the IC₅₀ (μM) 2) CETSA reported as concentration (μM) that induced half-maximum loss of luminescence (AC₅₀) compared to control. Percent (%) luminescence at the highest dose (100 μM) compared to control (DMSO). Target engagement (TE) reported as “Yes” if the ΔT_m difference from control at the highest dose was > control mean+3SD; otherwise, AC₅₀ not calculated (NC) and TE reported as “No”. 3) Reduction in the ratio pAKT/tAKT determined by Alpha SureFire assay and reported as the geometric mean of the IC₅₀ (μM). 4) Activation of BV2 cells and 5) HMC3 cells based on increased uptake of pHrodo myelin (EC₅₀). Cell health monitored as decreased cell count (IC₅₀) and decreased nuclear intensity (IC₅₀). Values reported as the geometric mean of the EC₅₀ or IC₅₀ (μM). NC = not calculated due to curve fitting error. NT = not tested.

destabilizing the protein. Thermal stabilization of SHIP1 was not observed with any SHIP1 inhibitors. Compounds that did not appear to engage SHIP1 by CETSA were inactive in secondary cellular assays or simply cytotoxic at high concentrations. Although some SHIP1 inhibitors appeared to engage the target in cells, they did not activate phagocytosis and at high concentrations were cytotoxic. Other compounds increased phagocytosis only at high concentrations likely due to cell stress. Some compounds appeared to induce early or late apoptosis at lower concentrations. All SHIP1 inhibitors reduced the ratio of pAKT/tAKT in THP1 cells and this reduction was correlated to cytotoxicity in BV2 and HMC3 suggesting reduced AKT signaling may be driving mechanisms of programmed cell death in these immortalized microglia-like cell lines. The reduced pAKT observed in THP1 cells is inconsistent with reports of increased AKT phosphorylation observed with SHIP1 inhibitors such as K116 in other cellular contexts⁴¹. The differences observed might indicate distinct signaling mechanisms through which PI(3,4,5)P₃ and PI(3,4)P₂

activate AKT signaling that are cell context dependent⁵⁶. Further studies with these compounds would be required to reconcile these differences in SHIP1-dependent AKT signaling.

Only compound **23** demonstrated target engagement by CETSA, reduced pAKT, and induced phagocytosis of both BV2 and HMC3 cells at concentrations that did not result in significant changes in either cell count or nuclear intensity. At high concentrations, compound **23** appeared to induce late apoptosis in BV2 cells and early apoptosis in HMC3 cells. Compound **23** also activated primary mouse microglia isolated from neonate mice. We can't rule out that these effects may also involve other targets or mechanisms, but this compound was unique in its consistency across assays, lack of cytotoxicity, and favorable physicochemical and ADME properties. Therefore, we advanced it to primary mouse microglia and *in vivo* PK studies in mice. Although compound **23** demonstrated significant exposures in both plasma and brain with a brain/plasma ratio of 0.5–3-fold that increased over time, it should be noted that high protein binding (see **Table 7**) may limit its ability to sufficiently engage SHIP1 *in vivo*. Similar to other SHIP1 inhibitors we assessed, compound **23** exhibits potency in the micromolar range, a level somewhat greater than the typical requirement for a clinical candidate for human studies. For most of the other SHIP1 inhibitors we evaluated, the combination of low potency and unfavorable chemical properties, such as poor solubility, poses significant challenges utilizing them as chemical tools for target validation. Compound **23** was unique in that its solubility and permeability, coupled with potency and relative lack of cytotoxicity, makes it a suitable lead-like molecule for a medicinal chemistry campaign to improve potency while maintaining drug-like properties. Therefore, SAR studies are being conducted by our team around compound **23** to improve potency at SHIP1 and induce phagocytosis without cytotoxicity while increasing free-fraction exposures *in vivo*. These studies will be reported elsewhere.

ACKNOWLEDGMENTS

The logistical and project management support of Ariel Bontrager at Purdue University is gratefully acknowledged. The authors are grateful for the resources and support of the University of Pittsburgh Preclinical Phenotyping Core (PPC). Mass spectrometry was provided by the Clinical Pharmacology Analytical Core (CPAC) at Indiana University School of Medicine. We gratefully thank Louise Pay for editing the manuscript.

CONFLICTS OF INTEREST

Adrian Oblak, Andrew Mesecar, Bruce Lamb, Alan Palkowitz and Timothy Richardson are consultants for Monument Biosciences. Bruce Lamb receives licensing fees from Ionis Pharmaceuticals. He participates on the Advisory Board and receives consulting fees from NervGen Inc. and The Cleveland Clinic. He has a leadership or fiduciary role at the Alzheimer's Association and Cure Alzheimer's Fund. He has received travel support from Alzheimer's Association and Cure Alzheimer's Fund, and Department of Defense. Alan Palkowitz is president and CEO of the Indiana Biosciences Research Institute. Timothy Richardson is an advisor for Enveda Biosciences. Sara Quinney received an honorarium from Thomas Jefferson University for a lecture. She participates on the Data Safety Monitoring Board for AHA funded and NIH funded studies relating to effect of steroid hormones on QTc prolongation and drug-drug interactions between CBD and tacrolimus. Stacey Sukoff Rizzo participates on the Data Safety Monitoring Board for the Alzheimer's Disease Cooperative Study, has received an honoraria for lectures from University of Wisconsin - Madison, Neumora Therapeutics, University of New Mexico, University of Texas San Antonio and University of South Florida, and travel support from Rainwater Charitable Foundation and the Alzheimer's Association. Cynthia Jesudason, Greg Durst, Philip Hipskind, Daniel Beck, Stacey Sukoff Rizzo, and Timothy Richardson disclose that they have patents planned or pending. All funding provided to the institution and individual authors has been disclosed in the funding information and the declaration of interest section. No other authors have conflict of interests to disclose.

FUNDING SOURCES

This research was supported by the National Institute for Aging of the National Institutes of Health under award U54 AG065181. KS was also supported by a Frederick N. Andrews graduate research fellowship. CPAC core facility supported by the IU Simon Comprehensive Cancer Center Support Grant P30 CA082709.

REFERENCES

1. Zhang B, Gaiteri C, Bodea LG, et al. Integrated systems approach identifies genetic nodes and networks in late-onset Alzheimer's disease. *Cell*. Apr 25 2013;153(3):707-20. doi:10.1016/j.cell.2013.03.030
2. Jin SC, Benitez BA, Karch CM, et al. Coding variants in TREM2 increase risk for Alzheimer's disease. *Hum Mol Genet*. Nov 1 2014;23(21):5838-46. doi:10.1093/hmg/ddu277
3. Kierdorf K, Erny D, Goldmann T, et al. Microglia emerge from erythromyeloid precursors via Pu.1- and Irf8-dependent pathways. *Nat Neurosci*. Mar 2013;16(3):273-80. doi:10.1038/nn.3318
4. Efthymiou AG, Goate AM. Late onset Alzheimer's disease genetics implicates microglial pathways in disease risk. *Mol Neurodegener*. May 26 2017;12(1):43. doi:10.1186/s13024-017-0184-x
5. Target Enablement to Accelerate Therapy Development for Alzheimer's Disease. Accessed January 16, 2022, <https://treatad.org/>
6. Richardson T, Jesudason C, Chu S, et al. IUSM-Purdue TREAT-AD Center Target Enabling Component; INPP5D (SHIP1) Chemical Probe. *Zenodo*. 2022;doi:10.5281/zenodo.7231788
7. Lambert JC, Ibrahim-Verbaas CA, Harold D, et al. Meta-analysis of 74,046 individuals identifies 11 new susceptibility loci for Alzheimer's disease. *Nat Genet*. Dec 2013;45(12):1452-8. doi:10.1038/ng.2802
8. INPP5D inositol polyphosphate-5-phosphatase D Nominated Target Accessed 12/30/2021, 2021. [https://agora.adknowledgeportal.org/genes/\(genes-router:gene-details/ENSG00000168918\)](https://agora.adknowledgeportal.org/genes/(genes-router:gene-details/ENSG00000168918))
9. Lin PBC, Tsai APY, Soni D, et al. *INPP5D* deficiency attenuates amyloid pathology in a mouse model of Alzheimer's disease. *Alzheimer's & Dementia*. 2022;doi:10.1002/alz.12849
10. Peng Q, Malhotra S, Torchia JA, Kerr WG, Coggeshall KM, Humphrey MB. TREM2- and DAP12-dependent activation of PI3K requires DAP10 and is inhibited by SHIP1. *Sci Signal*. May 18 2010;3(122):ra38. doi:10.1126/scisignal.2000500
11. Pauls SD, Marshall AJ. Regulation of immune cell signaling by SHIP1: A phosphatase, scaffold protein, and potential therapeutic target. *Eur J Immunol*. Jun 2017;47(6):932-945. doi:10.1002/eji.201646795
12. Ono M, Bolland S, Tempst P, Ravetch JV. Role of the inositol phosphatase SHIP in negative regulation of the immune system by the receptor Fc(gamma)RIIB. *Nature*. Sep 19 1996;383(6597):263-6. doi:10.1038/383263a0
13. Gratuze M, Leyns CEG, Holtzman DM. New insights into the role of TREM2 in Alzheimer's disease. *Mol Neurodegener*. Dec 20 2018;13(1):66. doi:10.1186/s13024-018-0298-9
14. Kulkarni B, Kumar D, Cruz-Martins N, Sellamuthu S. Role of TREM2 in Alzheimer's Disease: A Long Road Ahead. *Mol Neurobiol*. Oct 2021;58(10):5239-5252. doi:10.1007/s12035-021-02477-9
15. Damen JE, Liu L, Rosten P, et al. The 145-kDa protein induced to associate with Shc by multiple cytokines is an inositol tetrakisphosphate and phosphatidylinositol 3,4,5-trisphosphate 5-phosphatase. *Proc Natl Acad Sci U S A*. Feb 20 1996;93(4):1689-93. doi:10.1073/pnas.93.4.1689
16. Blunt MD, Ward SG. Pharmacological targeting of phosphoinositide lipid kinases and phosphatases in the immune system: success, disappointment, and new opportunities. *Front Immunol*. 2012;3:226. doi:10.3389/fimmu.2012.00226
17. Le Coq J, Camacho-Artacho M, Velazquez JV, et al. Structural basis for interdomain communication in SHIP2 providing high phosphatase activity. *Elife*. Aug 9 2017;6doi:10.7554/eLife.26640
18. Scheffzek K, Welte S. Pleckstrin homology (PH) like domains - versatile modules in protein-protein interaction platforms. *FEBS Lett*. Aug 14 2012;586(17):2662-73. doi:10.1016/j.febslet.2012.06.006
19. Ono M, Okada H, Bolland S, Yanagi S, Kurosaki T, Ravetch JV. Deletion of SHIP or SHP-1 reveals two distinct pathways for inhibitory signaling. *Cell*. Jul 25 1997;90(2):293-301. doi:10.1016/s0092-8674(00)80337-2
20. Zhang J, Ravichandran KS, Garrison JC. A key role for the phosphorylation of Ser440 by the cyclic AMP-dependent protein kinase in regulating the activity of the Src homology 2 domain-containing Inositol 5'-phosphatase (SHIP1). *J Biol Chem*. Nov 5 2010;285(45):34839-49. doi:10.1074/jbc.M110.128827

21. Tsai AP, Lin PB, Dong C, et al. INPP5D expression is associated with risk for Alzheimer's disease and induced by plaque-associated microglia. *Neurobiol Dis*. Jun 2021;153:105303. doi:10.1016/j.nbd.2021.105303
22. Bunnage ME, Chekler ELP, Jones LH. Target validation using chemical probes. *Nature Chemical Biology*. 2013;9(4):195-199. doi:10.1038/nchembio.1197
23. Zhang Z-Y, Putt K, Chu S, et al. IUSM-Purdue TREAT-AD Center Target Enablement Resource; INPP5D (SHIP1) Screening. *Zenodo*. 2022;doi:10.5281/zenodo.6208450
24. Bradshaw W, Priestley R, Obst J, Hall-Roberts H, Cederbalk A, Brennan P. SH2-containing-inositol-5-phosphatases (INPP5D); A Target Enabling Package. *Zenodo*. 2020;doi:10.5281/zenodo.4429248
25. Viernes DR, Choi LB, Kerr WG, Chisholm JD. Discovery and development of small molecule SHIP phosphatase modulators. *Med Res Rev*. Jul 2014;34(4):795-824. doi:10.1002/med.21305
26. Schwaid AG, Cornella-Taracido I. Causes and Significance of Increased Compound Potency in Cellular or Physiological Contexts. *J Med Chem*. Mar 8 2018;61(5):1767-1773. doi:10.1021/acs.jmedchem.7b00762
27. Yu V, Pistillo J, Archibeque I, et al. Differential selectivity of JAK2 inhibitors in enzymatic and cellular settings. *Exp Hematol*. May 2013;41(5):491-500. doi:10.1016/j.exphem.2013.01.005
28. Carter SG, Karl DW. Inorganic phosphate assay with malachite green: an improvement and evaluation. *J Biochem Biophys Methods*. Dec 1982;7(1):7-13. doi:10.1016/0165-022x(82)90031-8
29. Pegan SD, Tian Y, Sershon V, Mesecar AD. A universal, fully automated high throughput screening assay for pyrophosphate and phosphate release from enzymatic reactions. *Comb Chem High Throughput Screen*. Jan 2010;13(1):27-38. doi:10.2174/138620710790218203
30. Bosshart H, Heinzelmann M. THP-1 cells as a model for human monocytes. *Ann Transl Med*. Nov 2016;4(21):438. doi:10.21037/atm.2016.08.53
31. Baran CP, Tridandapani S, Helgason CD, Humphries RK, Krystal G, Marsh CB. The inositol 5'-phosphatase SHIP-1 and the Src kinase Lyn negatively regulate macrophage colony-stimulating factor-induced Akt activity. *J Biol Chem*. Oct 3 2003;278(40):38628-36. doi:10.1074/jbc.M305021200
32. Mason ER, Soni DM, Chu S. Microglial Phagocytosis/Cell Health High-Content Assay. *Curr Protoc*. Mar 2023;3(3):e724. doi:10.1002/cpz1.724
33. Bradshaw WJ, Newman JA, von Delft F, et al. INPP5D PanDDA analysis group deposition -- Crystal Structure of the phosphatase and C2 domains of SHIP1 in complex with Z1348371854. *Protein Data Bank*. 2020;doi:10.2210/pdb5RWL/pdb
34. Zhang H, He J, Kutateladze TG, et al. 5-Stabilized phosphatidylinositol 3,4,5-trisphosphate analogues bind Grp1 PH, inhibit phosphoinositide phosphatases, and block neutrophil migration. *Chembiochem*. Feb 15 2010;11(3):388-95. doi:10.1002/cbic.200900545
35. Vandeput F, Combettes L, Mills SJ, et al. Biphenyl 2,3',4,5',6-pentakisphosphate, a novel inositol polyphosphate surrogate, modulates Ca²⁺ responses in rat hepatocytes. *FASEB J*. May 2007;21(7):1481-91. doi:10.1096/fj.06-7691com
36. Brooks R, Fuhler GM, Iyer S, et al. SHIP1 inhibition increases immunoregulatory capacity and triggers apoptosis of hematopoietic cancer cells. *J Immunol*. Apr 1 2010;184(7):3582-9. doi:10.4049/jimmunol.0902844
37. Fuhler GM, Brooks R, Toms B, et al. Therapeutic potential of SH2 domain-containing inositol-5'-phosphatase 1 (SHIP1) and SHIP2 inhibition in cancer. *Mol Med*. Feb 10 2012;18:65-75. doi:10.2119/molmed.2011.00178
38. Kerr WG, Pedicone C, Dormann S, Pacherille A, Chisholm JD. Small molecule targeting of SHIP1 and SHIP2. *Biochem Soc Trans*. Feb 28 2020;48(1):291-300. doi:10.1042/BST20190775
39. Pedicone C, Meyer ST, Chisholm JD, Kerr WG. Targeting SHIP1 and SHIP2 in Cancer. *Cancers (Basel)*. Feb 20 2021;13(4)doi:10.3390/cancers13040890
40. Kerr W, Pedicone C, Chisolm JD, Dormann SM, inventors; Methods of Activating Microglial Cells. WO2020028552.
41. Pedicone C, Fernandes S, Dungan OM, et al. Pan-SHIP1/2 inhibitors promote microglia effector functions essential for CNS homeostasis. *J Cell Sci*. Jan 10 2020;133(5)doi:10.1242/jcs.238030
42. Suwa A, Yamamoto T, Sawada A, et al. Discovery and functional characterization of a novel small molecule inhibitor of the intracellular phosphatase, SHIP2. *Br J Pharmacol*. Oct 2009;158(3):879-87. doi:10.1111/j.1476-5381.2009.00358.x
43. Suwa A, Kurama T, Yamamoto T, Sawada A, Shimokawa T, Aramori I. Glucose metabolism activation by SHIP2 inhibitors via up-regulation of GLUT1 gene in L6 myotubes. *European journal of pharmacology*. 2010;642(1-3):177-182.

44. Annis DA, Cheng CC, Chuang CC, et al. Inhibitors of the lipid phosphatase SHIP2 discovered by high-throughput affinity selection-mass spectrometry screening of combinatorial libraries. *Comb Chem High Throughput Screen*. Sep 2009;12(8):760-71. doi:10.2174/138620709789104870
45. Ichihara Y, Fujimura R, Tsuneki H, et al. Rational design and synthesis of 4-substituted 2-pyridin-2-ylamides with inhibitory effects on SH2 domain-containing inositol 5'-phosphatase 2 (SHIP2). *Eur J Med Chem*. Apr 2013;62:649-60. doi:10.1016/j.ejmech.2013.01.014
46. Lim JW, Kim SK, Choi SY, et al. Identification of crizotinib derivatives as potent SHIP2 inhibitors for the treatment of Alzheimer's disease. *Eur J Med Chem*. Sep 5 2018;157:405-422. doi:10.1016/j.ejmech.2018.07.071
47. Seashore-Ludlow B, Axelsson H, Almqvist H, Dahlgren B, Jonsson M, Lundback T. Quantitative Interpretation of Intracellular Drug Binding and Kinetics Using the Cellular Thermal Shift Assay. *Biochemistry*. Dec 4 2018;57(48):6715-6725. doi:10.1021/acs.biochem.8b01057
48. Robers MB, Friedman-Ohana R, Huber KVM, et al. Quantifying Target Occupancy of Small Molecules Within Living Cells. *Annu Rev Biochem*. Jun 20 2020;89:557-581. doi:10.1146/annurev-biochem-011420-092302
49. Tolvanen TA. Current Advances in CETSA. *Front Mol Biosci*. 2022;9:866764. doi:10.3389/fmolb.2022.866764
50. Martinez NJ, Asawa RR, Cyr MG, et al. A widely-applicable high-throughput cellular thermal shift assay (CETSA) using split Nano Luciferase. *Sci Rep*. Jun 21 2018;8(1):9472. doi:10.1038/s41598-018-27834-y
51. Oh-Hashi K, Furuta E, Fujimura K, Hirata Y. Application of a novel HiBiT peptide tag for monitoring ATF4 protein expression in Neuro2a cells. *Biochem Biophys Rep*. Dec 2017;12:40-45. doi:10.1016/j.bbrep.2017.08.002
52. Singh N, Reyes-Ordóñez A, Compagnone MA, et al. Redefining the specificity of phosphoinositide-binding by human PH domain-containing proteins. *Nat Commun*. Jul 15 2021;12(1):4339. doi:10.1038/s41467-021-24639-y
53. Eramo MJ, Mitchell CA. Regulation of PtdIns(3,4,5)P3/Akt signalling by inositol polyphosphate 5-phosphatases. *Biochem Soc Trans*. Feb 2016;44(1):240-52. doi:10.1042/BST20150214
54. Scheid MP, Huber M, Damen JE, et al. Phosphatidylinositol (3,4,5)P3 is essential but not sufficient for protein kinase B (PKB) activation; phosphatidylinositol (3,4)P2 is required for PKB phosphorylation at Ser-473: studies using cells from SH2-containing inositol-5-phosphatase knockout mice. *J Biol Chem*. Mar 15 2002;277(11):9027-35. doi:10.1074/jbc.M106755200
55. Sohlenius-Sternbeck AK, Terelius Y. Evaluation of ADMET Predictor(TM) in early discovery DMPK project work. *Drug Metab Dispos*. Nov 8 2021;doi:10.1124/dmd.121.000552
56. Manning BD, Toker A. AKT/PKB Signaling: Navigating the Network. *Cell*. Apr 20 2017;169(3):381-405. doi:10.1016/j.cell.2017.04.001
57. Iversen PW, Eastwood BJ, Sittampalam GS, Cox KL. A comparison of assay performance measures in screening assays: signal window, Z' factor, and assay variability ratio. *J Biomol Screen*. Apr 2006;11(3):247-52. doi:10.1177/1087057105285610
58. Eastwood BJ, Farmen MW, Iversen PW, et al. The minimum significant ratio: a statistical parameter to characterize the reproducibility of potency estimates from concentration-response assays and estimation by replicate-experiment studies. *J Biomol Screen*. Apr 2006;11(3):253-61. doi:10.1177/1087057105285611
59. Gad SC, Spainhour CB, Shoemaker C, et al. Tolerable Levels of Nonclinical Vehicles and Formulations Used in Studies by Multiple Routes in Multiple Species With Notes on Methods to Improve Utility. *Int J Toxicol*. Mar-Apr 2016;35(2):95-178. doi:10.1177/1091581815622442
60. Thackaberry EA, Kopytek S, Sherratt P, Trouba K, McIntyre B. Comprehensive investigation of hydroxypropyl methylcellulose, propylene glycol, polysorbate 80, and hydroxypropyl-beta-cyclodextrin for use in general toxicology studies. *Toxicol Sci*. Oct 2010;117(2):485-92. doi:10.1093/toxsci/kfq207
61. Fernandes S, Meyer ST, Shah JP, Adhikari AA, Kerr WG, Chisholm JD. N1-Benzyl Tryptamine Pan-SHIP1/2 Inhibitors: Synthesis and Preliminary Biological Evaluation as Anti-Tumor Agents. *Molecules*. Dec 2 2022;27(23)doi:10.3390/molecules27238451